# EO-1/Hyperion: Nearing Fourteen Years of Successful Mission Science Operation and End of Mission Plans

**Elizabeth M. Middleton**

**EO-1 Mission Scientist 2007- present**

**Biospheric Sciences Laboratory, NASA GSFC**

**July, 2014**


**IGARSS 2014**
**Québec City**
**Québec, Canada**

NASA

# EO-1/Hyperion: Nearing Fourteen Years of Successful Mission Science Operation and End of Mission Plans


Elizabeth M. Middleton

*NASA/Goddard Space Flight Center, Greenbelt, Maryland, USA*

*With….*

Daniel J. Mandl, *Mission Manager, NASA/GSFC, Greenbelt, MD*

Stuart W. Frye, *SGT, Greenbelt, MD*

Lawrence Ong, *Systems Science & Applications, Inc., Lanham, MD*

Stephen G. Ungar, *Former Mission Scientist, USRA, Columbia, MD*

Petya E. Campbell & K. Fred Huemmrich, *University of MD Baltimore Co., Baltimore, MD*

David R. Landis, *Sigma Space Corp., Inc., Lanham, MD*

Robert O. Green, *Jet Propulsion Lab, Pasadena, California*

# EO-1 on the Pad

November 2000

# Hyperion Imaging Spectrometer

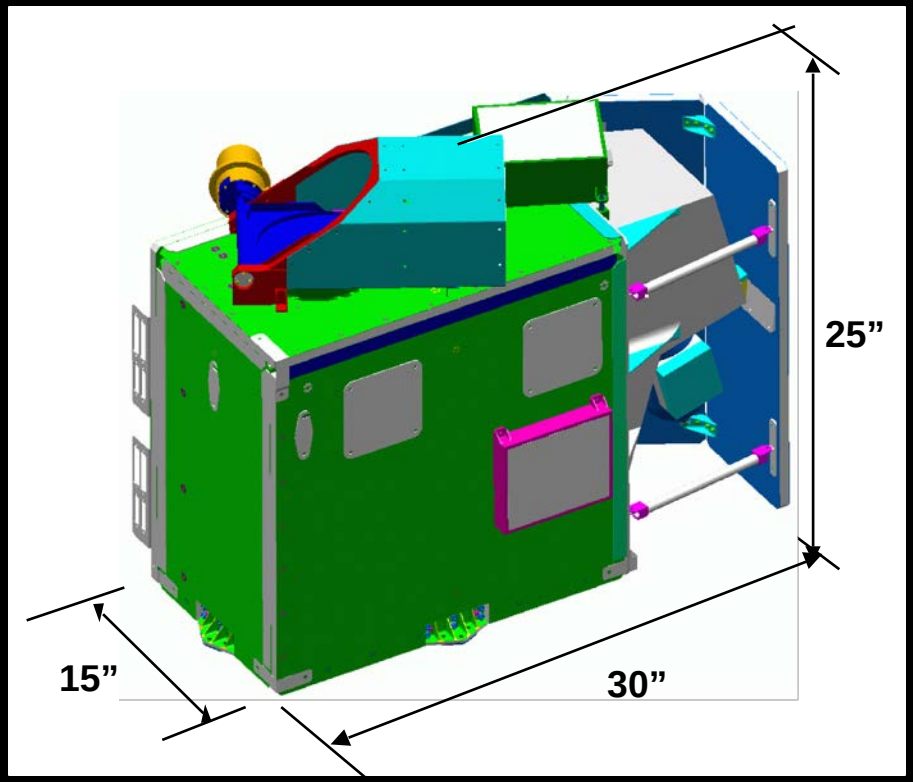


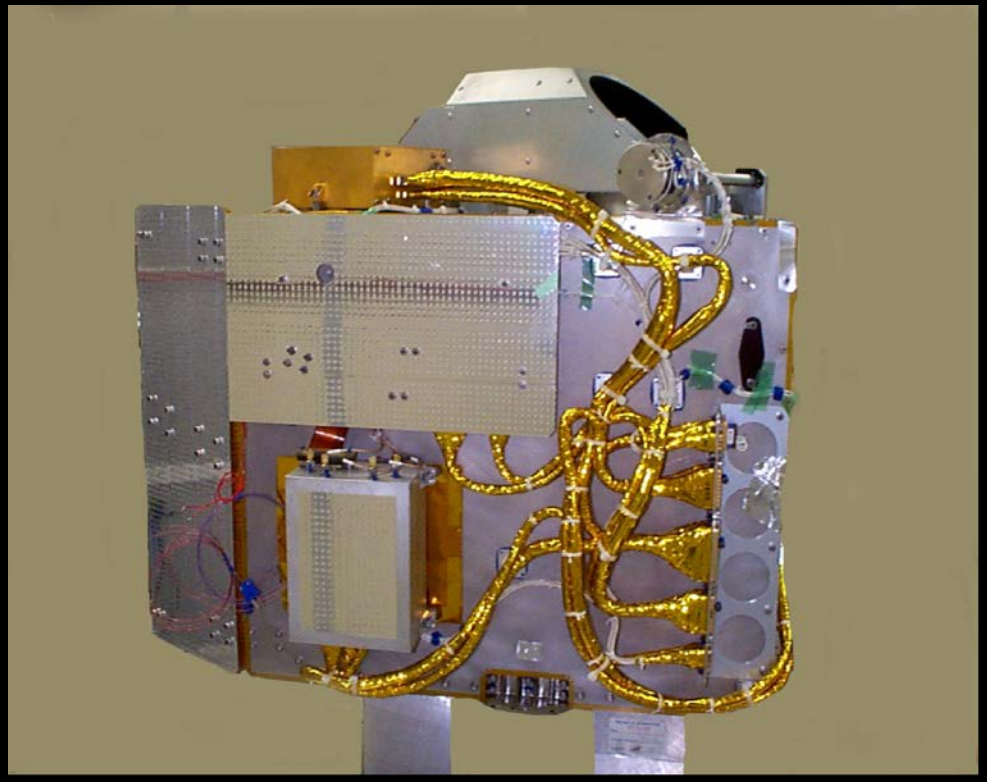

**Hyperion is a push-broom imager**

- 220 10nm bands covering 400nm - 2500nm
- 6% absolute rad. accuracy
- Swath width of 7.5 km
- IFOV of 42.4 μradian
- GSD of 30 m
- 12-bit image data
- Orbit is 705km alt (16 day repeat)

- Convex Grating spectrometers with CCD VNIR and HgCdTe SWIR detectors (60μm pixels)
- 30m spatial and 10nm spectral resolutions over 7.5km swath and 400-2500nm spectral range
- Multiple calibration options: lamps, lunar, solar, ground imaging and laboratory
- Hyperspectral Imaging Capability to address Earth Observation applications

# Hyperion Optical System

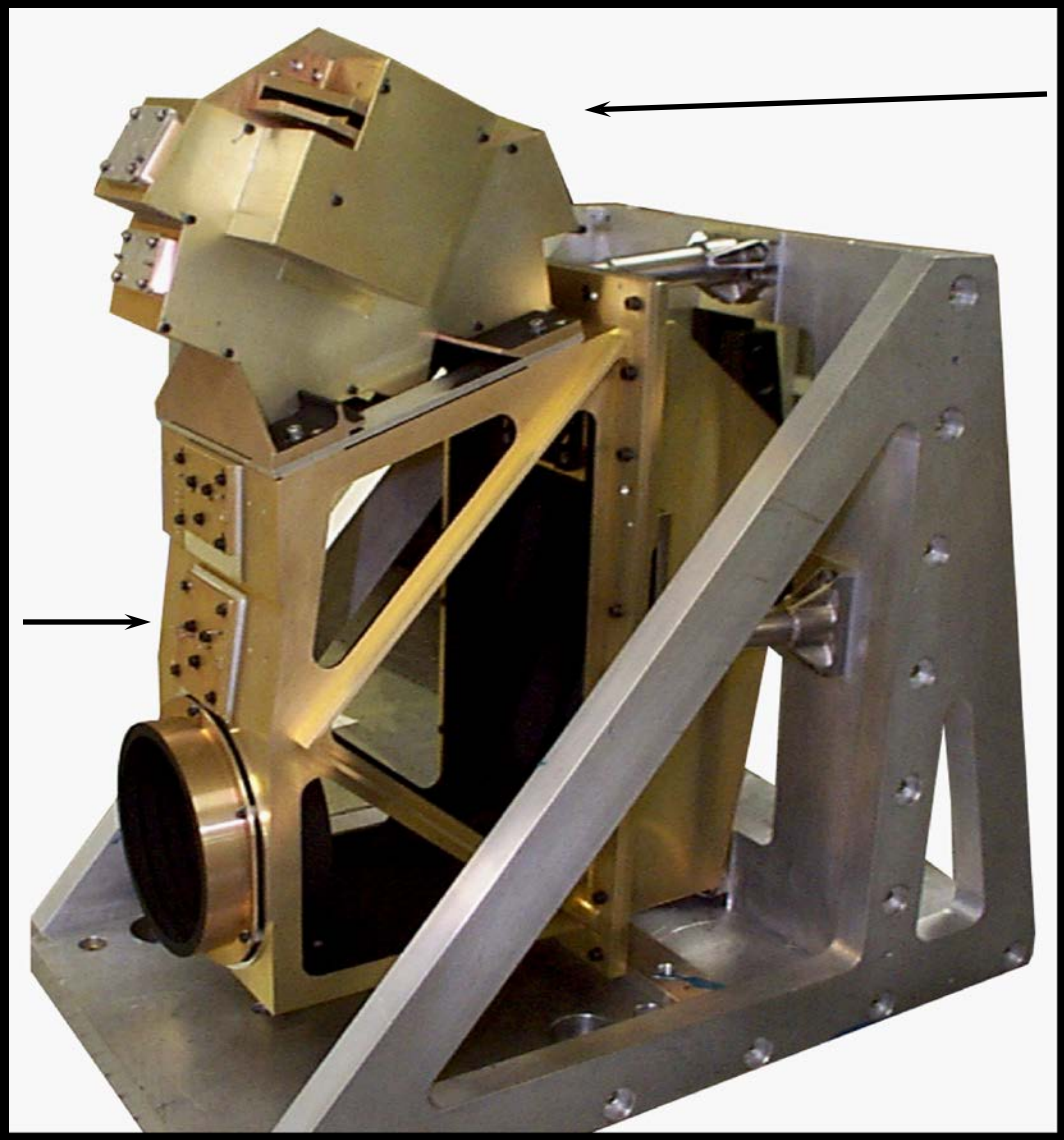

# Earth Observing-1 (EO-1) Mission

*Mission Scientist, Dr. Elizabeth Middleton (NASA/GSFC Code 618)*
*Mission Manager, Mr. Daniel Mandl (NASA/GSFC Code 581)*

**EO-1 was designed to flight validate technologies and operational approaches applicable to future Earth observing missions. Launched on November 21, 2000, it is currently in its 14th year, with more than 150,000 scenes in archive.**

http://eo1.gsfc.nasa.gov/

| ALI | | Hyperion |
|---|---|---|
| **Band Designations** | **Band Names (wavelength, μm)** | |
| Pan | Pan (0.48 – 0.69) | Continuous Spectra 0.4 – 2.4 μm 242 Bands Bandwidth: 10nm |
| Blue | MS-1p (0.433 – 0.453) | |
| | MS-1 (0.450 – 0.515) | |
| Green | MS-2 (0.525 – 0.605) | |
| Red | MS-3 (0.633 – 0.690) | |
| NIR | MS-4 (0.775 – 0.805) | |
| | MS-4p (0.845 – 0.890) | |
| SWIR | MS-5p (1.20 – 1.30) | |
| | MS-5 (1.55 – 1.75) | |
| | MS-7 (2.08 – 2.35) | |
| Spatial Resolution | Pan: 10m, MS: 30m | 30m |
| Swath Width | 37km | 7.7km |

# EO-1 and Landsat 7
# Descending Orbit Ground Tracks

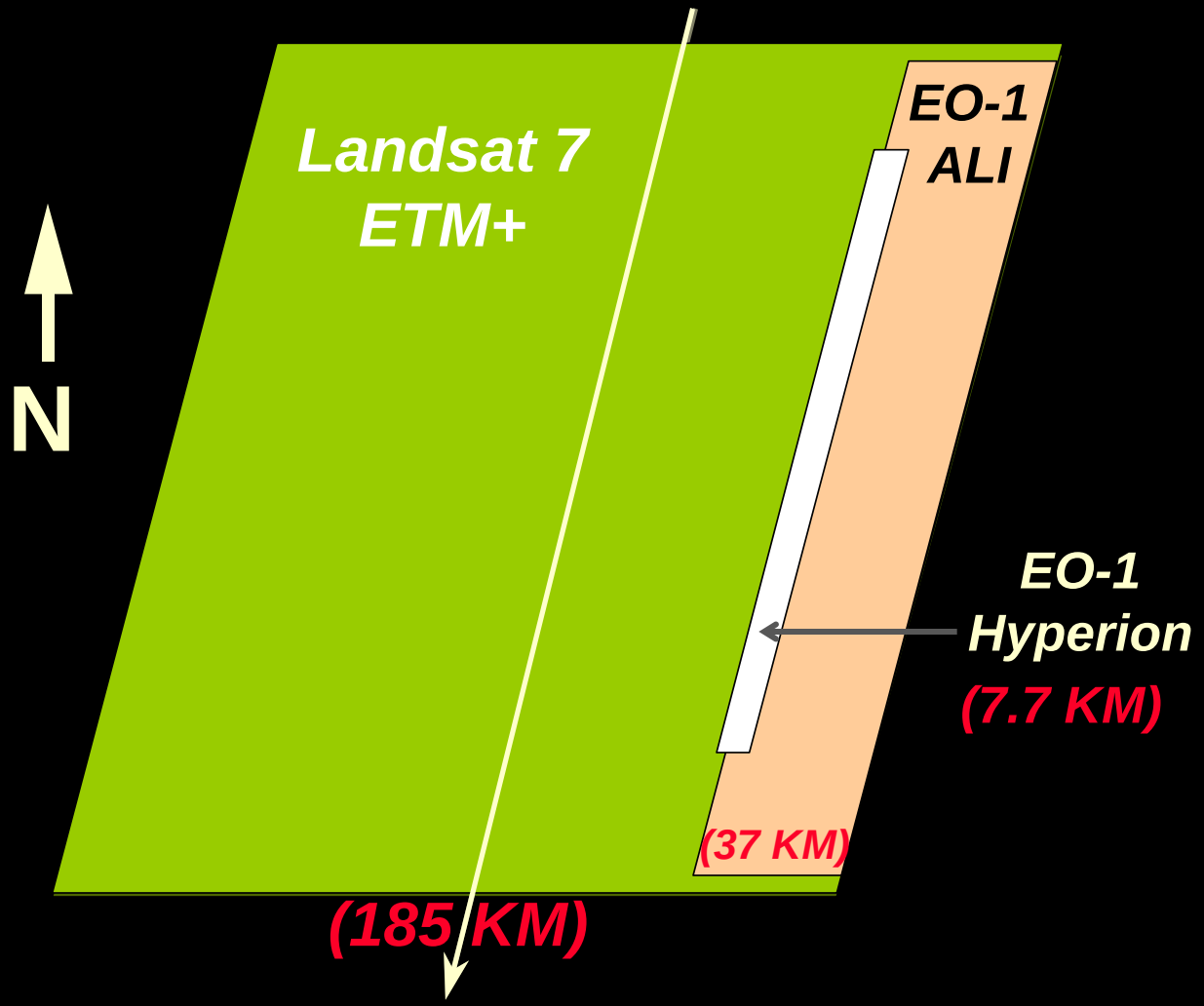

# Measuring the Global Terrestrial Biosphere for Ecosystem Composition and Function

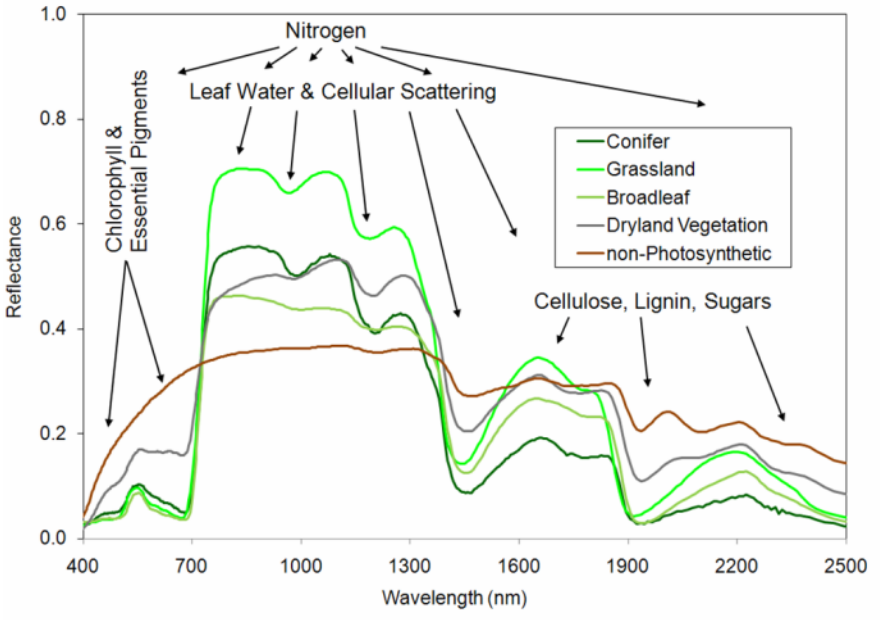


Imaging Spectroscopy is required to measure critical variables of the terrestrial biosphere.

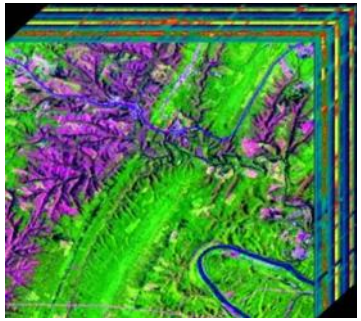

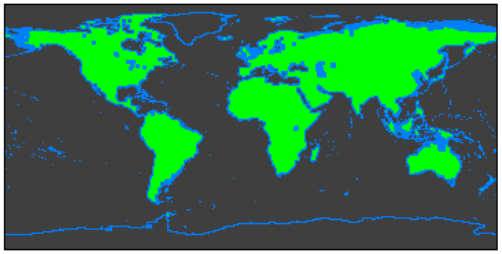

Multi-spectral imaging is insufficient

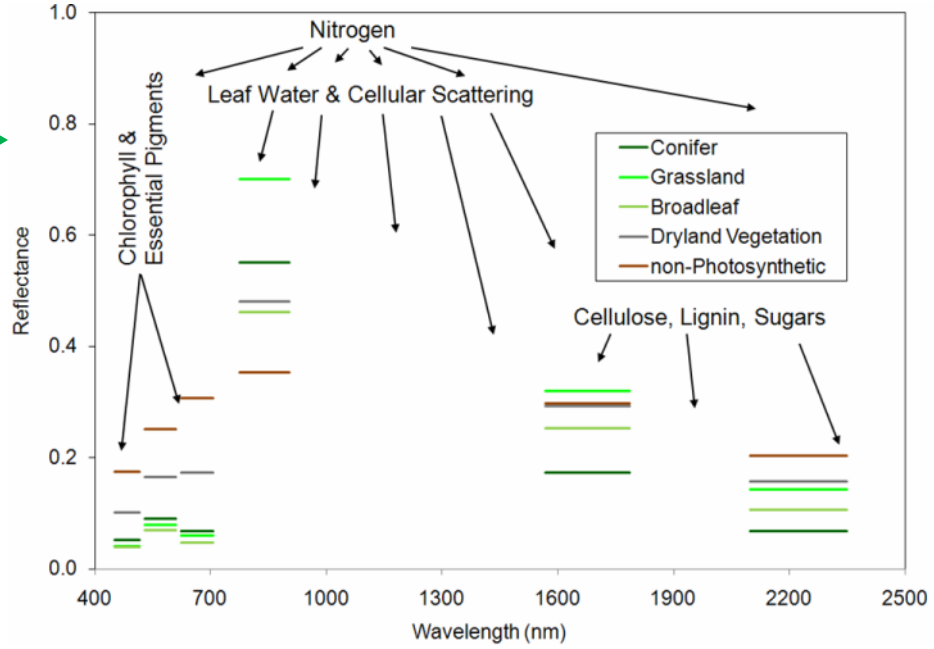

# Hyperion Images from July 2014

July 1, 2014
Hyperion False-Color Image
Nitmiluk National Park, Australia

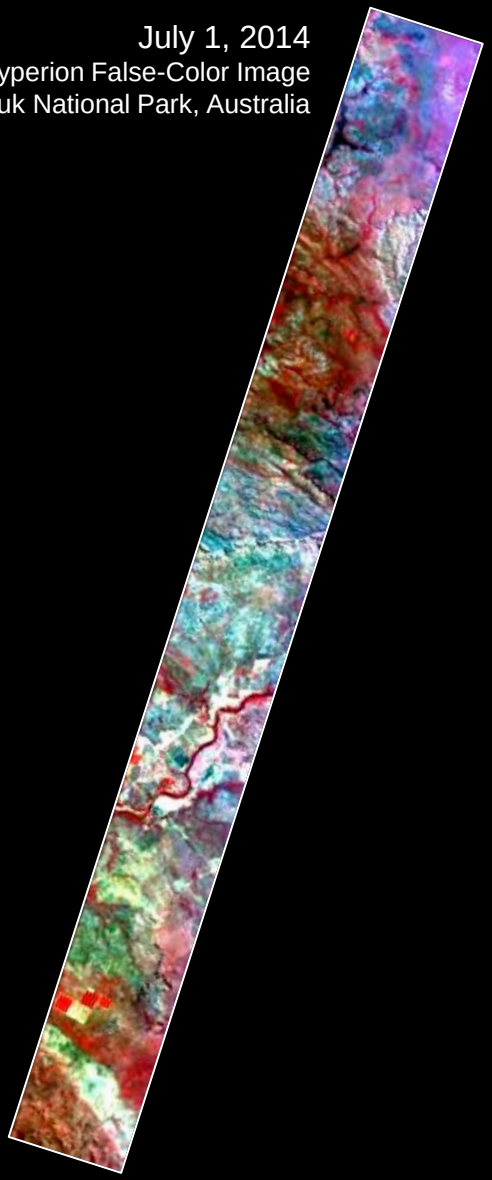

July 5, 2014
Hyperion False-Color Image
Mato Grosso, Brazil

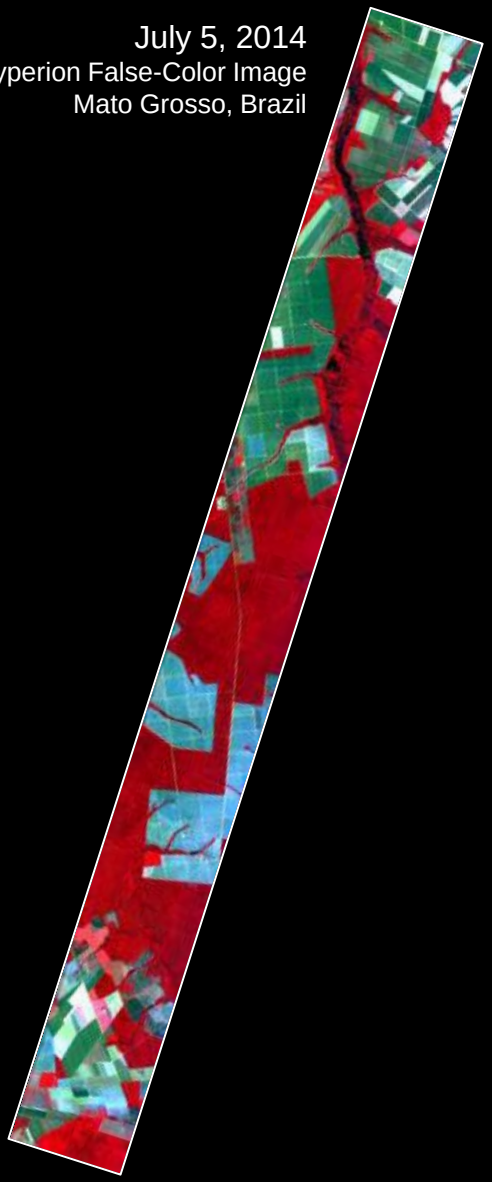

July 8, 2014
Hyperion False-Color Image
Port-au-Prince, Haiti

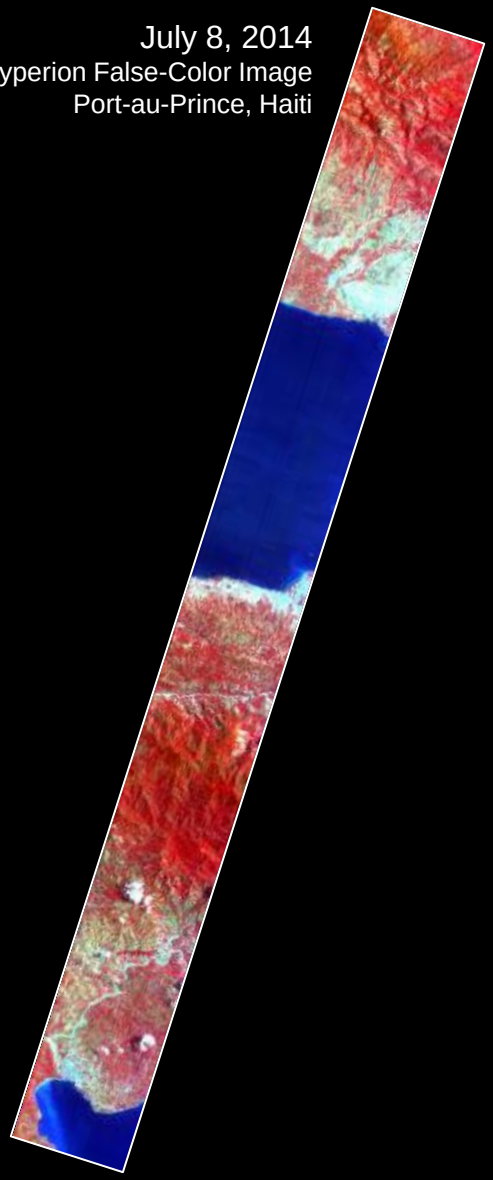

# Skiing in Sochi, Russia

February 8, 2014
True-Color Image from ALI
Skiing in Sochi, Russia

While Sochi is a coastal town on the Black Sea, the skiing events for the XXII Winter Olympic Games took place about 25 miles inland. The venues were clustered around Krasnaya Polyana, a small town tucked between the Aibiga and Psekhako Ridges in the western Caucasus.

The Rosa Khutor Alpine Center is the home to the downhill, snowboard, and freestyle events. The combined downhill skiing area measures about 12 miles in total, with the men's downhill course stretching 11,482 feet and featuring a 3,526 foot change in elevation. The highest lift climbs to the summit of Rosa Peak, which rises 7,612 feet.

The same steep slopes that make Rosa Peak good for skiing also elevate the risk of avalanches. To protect against falling snow, planners installed a series of gas pipes along the top of the ridge. The pipes emit bursts of oxygen and propane that create small, controlled avalanches. Event organizers also installed a series of earthen dams to steer snow away from infrastructure, and they have deployed two backhoes to the top of Aibiga Ridge to knock cornices away before they pose a risk.

# Recent Major Events for EO-1

- February 2011: EO-1 ran out of fuel and began precession from 10:00am overpass toward earlier times.
- June 2012: started new lunar calibration scans that use Hyperion.
- April 6, 2012: EO-1 “Safe Hold” incident. This was our first major "safe hold" and there was no guarantee that the satellite would come back up. But the restart procedures worked properly and 2 weeks later EO-1 was working fine.
- March 2013: Senior Review proposal delivered to NASA HQ, resulting in 2 more years of funding.
- May 2013: IEEE JSTARS EO-1 Special Issue published, containing 20 papers.
- December 18, 2013: EO-1 “Safe Hold” incident, caused by a "low power" reading. EO-1 was restarted and the "low power" level was set higher.
- May 9, 2014: a piece of Chinese space debris had a chance of impacting the EO-1 satellite, so a 10-second thruster burn was attempted (without knowing if it would work). The thrusters fired correctly, shifting EO-1 into a slightly higher orbit, avoiding the collision.
- October 2015: EO-1 is scheduled to be shut down.

# 2013 NASA Senior Review
# Earth Observing-1 (EO-1) Proposal

*Submitted by:*
**Mission Scientist, Dr. Elizabeth Middleton**
**Mission Manager, Mr. Daniel Mandl**

**May 1, 2013**

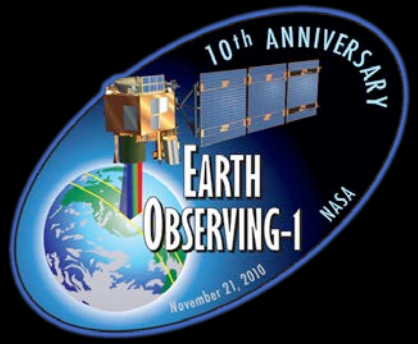


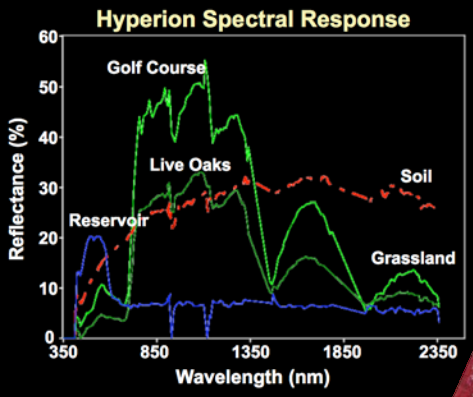


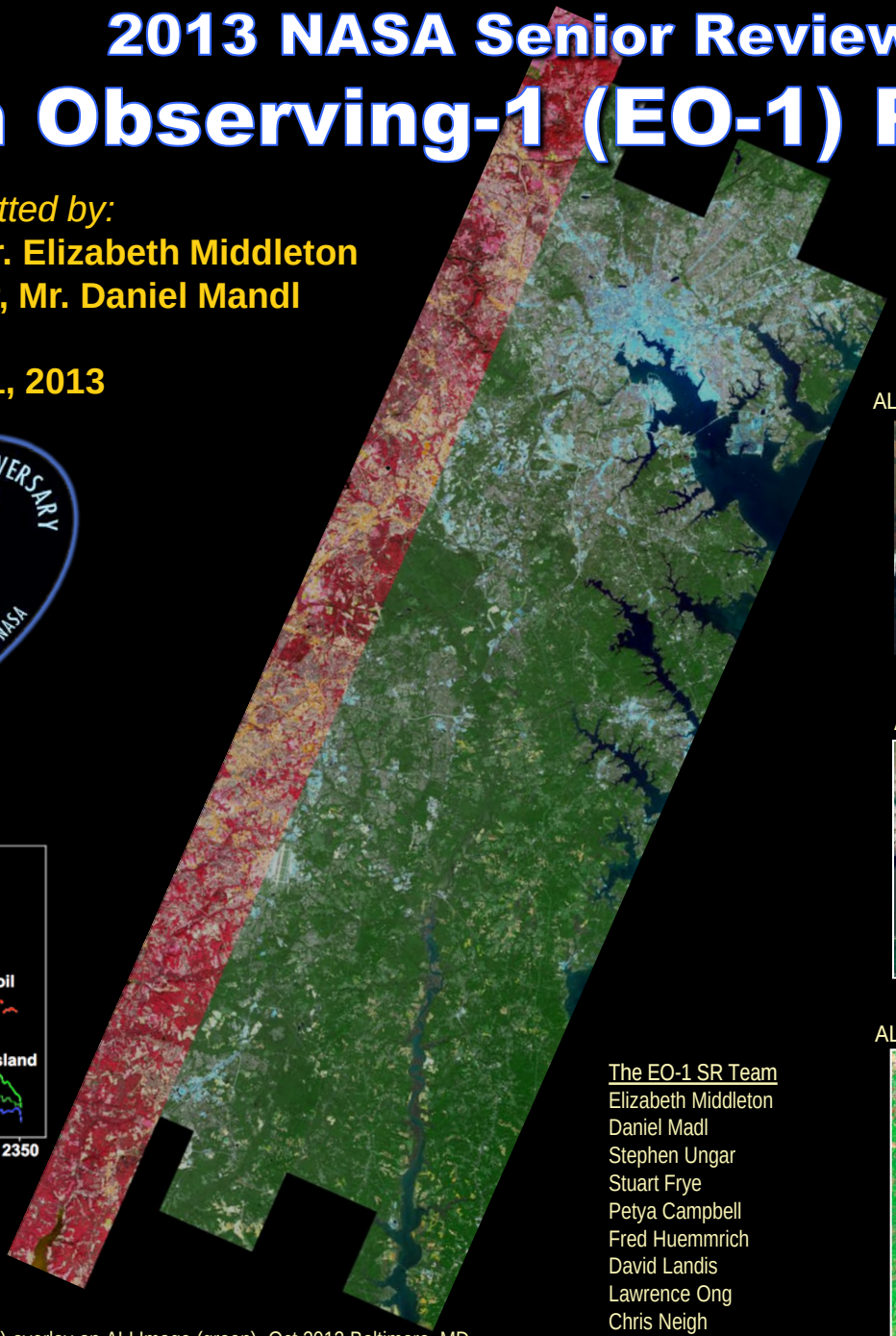

Hyperion (red) overlay on ALI Image (green), Oct 2012 Baltimore, MD

ALI False-Color Image, 2011 Lava Flows at Nabro Volcano

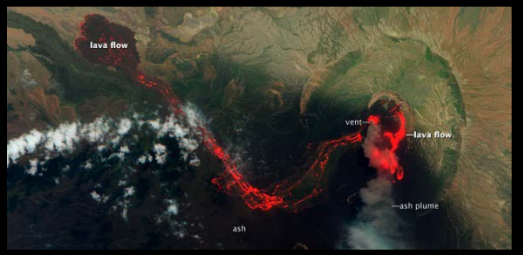


ALI True-Color Image, 2012 Low Water on Mississippi


ALI False-Color Image, 2012 Fire-Charred Forest in Mexico


The EO-1 SR Team
Elizabeth Middleton
Daniel Madl
Stephen Ungar
Stuart Frye
Petya Campbell
Fred Huemmrich
David Landis
Lawrence Ong
Chris Neigh

# AVIRIS/Hyperion Calibration

AVIRIS supported Hyperion cal/val during the EO-1 post-launch Argentina Field Campaign in Jan-Feb 2001. Currently, Hyperion and AVIRIS are being jointly used in support of the 2013-2014 HyspIRI Airborne Campaign in California.

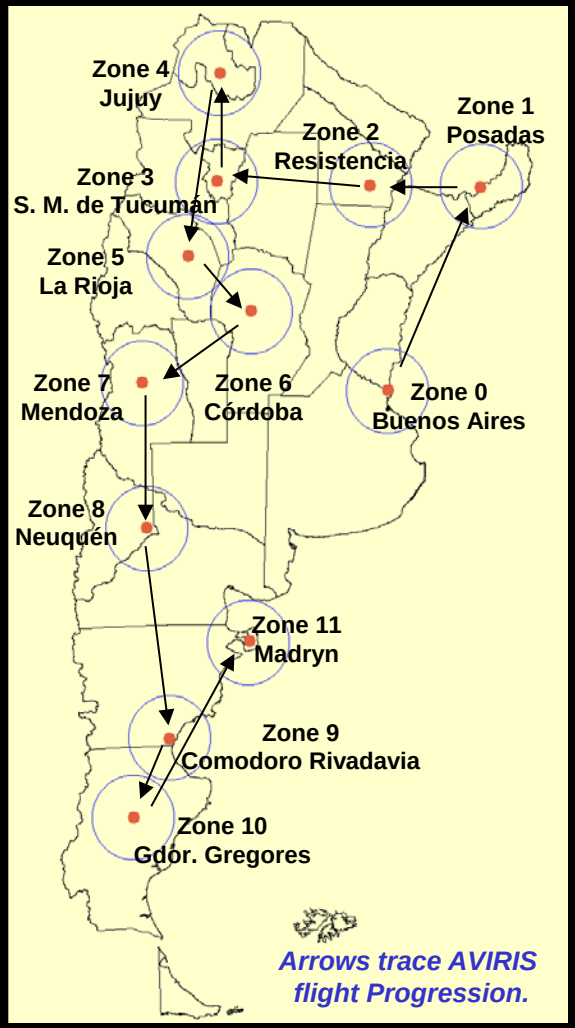


## The HyspIRI Airborne Campaign

***AVIRIS and Hyperion Overflights, April 2013, CA***


Hyperion (colored bars) is currently being used along with AVIRIS (red lines are AVIRIS flightlines) in support of the HyspIRI Airborne Campaign.

# ER-2 HyspIRI 2013 Operations & 2014 Plans

## Objectives

Conduct ER-2 Remote Sensing Missions with AVIRIS and MASTER over 6 regions for two years with measurements during Spring, Summer, and Fall.

## CY2013 Operations

- All CY2013 planned data was collected
- Station and Rim fire data added to the plan
- 121.8 total HyspIRI flight hours
- Obtained Landsat 8 underpass, Monterrey Bay, and Yosemite/Neon box data through other funded flight requests
- Provided piggyback opportunity for AirMSPI, RSP, NAST-I, NAST-M, S-HIS, and DCS

## CY2014 Flight Dates:

- Mar 31 – May 2
- May 27 – June 20
- Aug 18 – 29
- Sept 15 – Oct 31

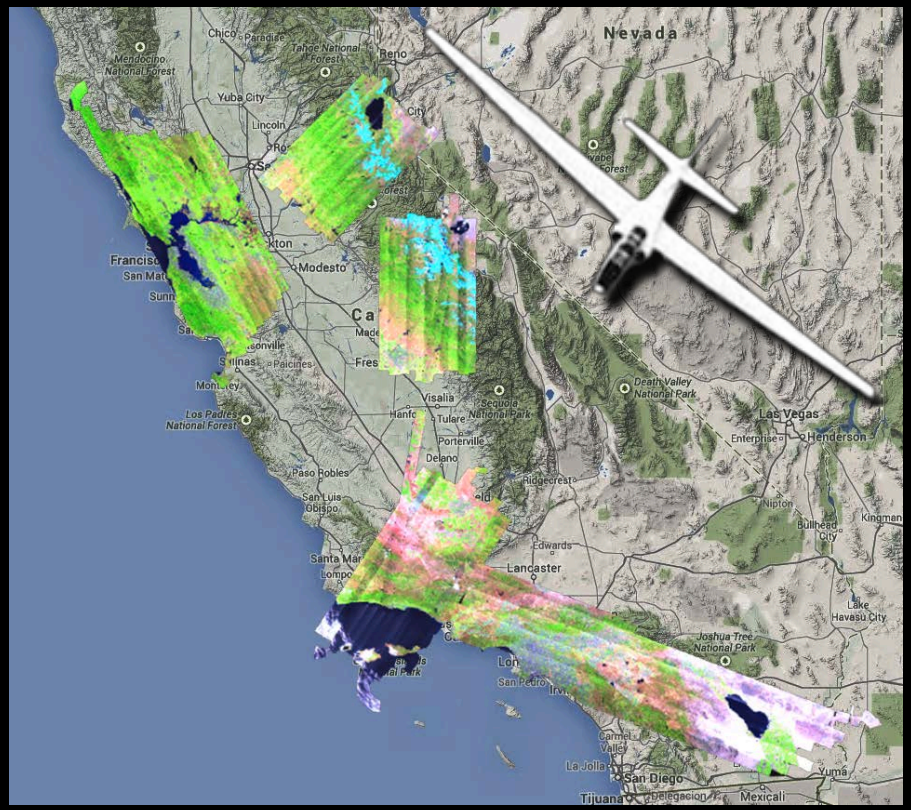


## CY2014 Plans

| Flight Request | Study Name | Flight Hours | Principal Investigator |
|---|---|---|---|
| 142016 | HyspIRI | 98.2 | Rob Green |
| 142020 | Landsat 8 | 8 | Rob Green |
| 142006 | ACOCO | 14.2 | Brian Cairns |
| 142007 | Precision Agriculture | 9 | Darren Drewry |

# EO-1 Scene Statistics

| | |
|---|---|
| Total ALI Scenes | 74,506 |
| Total Hyperion Scenes | 74,328 |
| Total Scenes Available | **148,834** |

**As of June 2014**

# EO-1 Acquisitions Global Distribution

## as of June 2014

EO-1 observations in 13 years (2001 through 2014) total over 75,000 for each instrument. Locations of collections made in 2011-2012 (1300+ per instrument) are shown with yellow dots, whereas those collected during the first 10 years are shown with red dots. In addition, locations of 4 repetitively observed sites are highlighted: CEOS calibration sites (blue circles), MSO (dark green circles), NEON (cyan circles) and Volcanoes (purple diamonds). Locations having >10 collects are outlined with black circles.

# Hyperion Product Usage

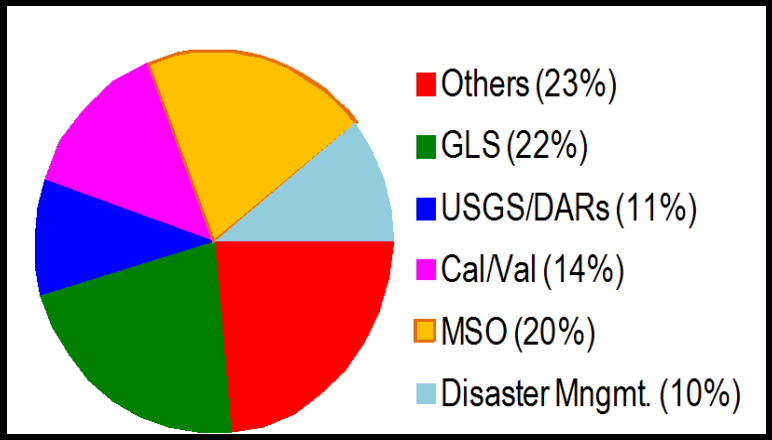


Distribution of scene requests by user categories: GLS = Global Land Surveys; MSO = Mission Science Office, Others include Volcanoes, SensorWebs, and IPM testing.

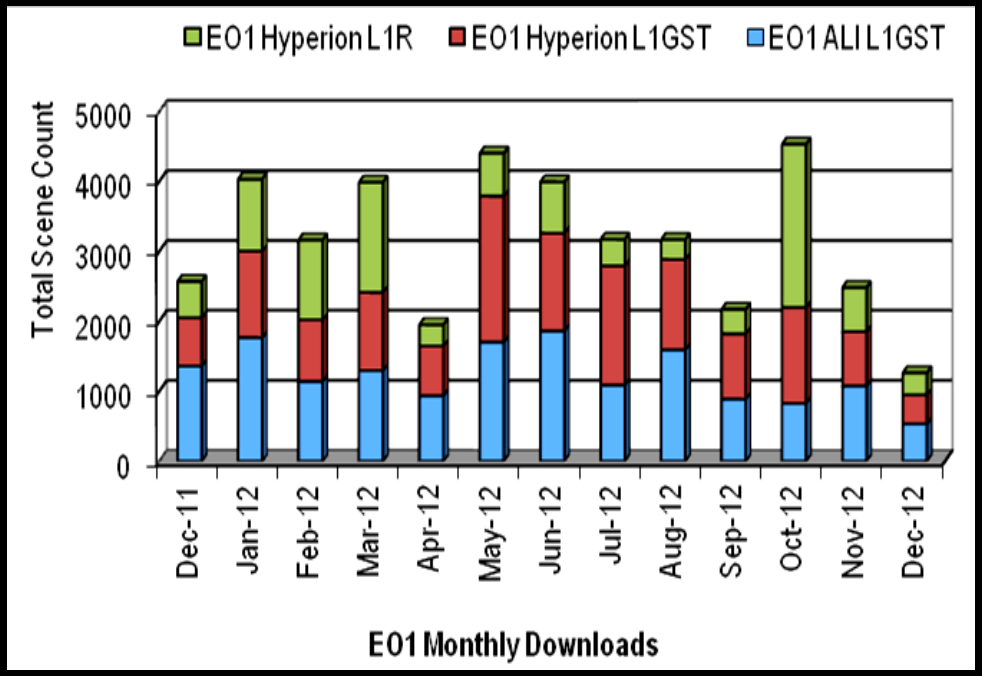


EO-1 Product Web-downloads from USGS in 2012.

# Hyperion's Long-Term Stability

The EO-1 Mission validates the long term stability of Hyperion by several methods, including comparing the Hyperion lamp and solar response changes.

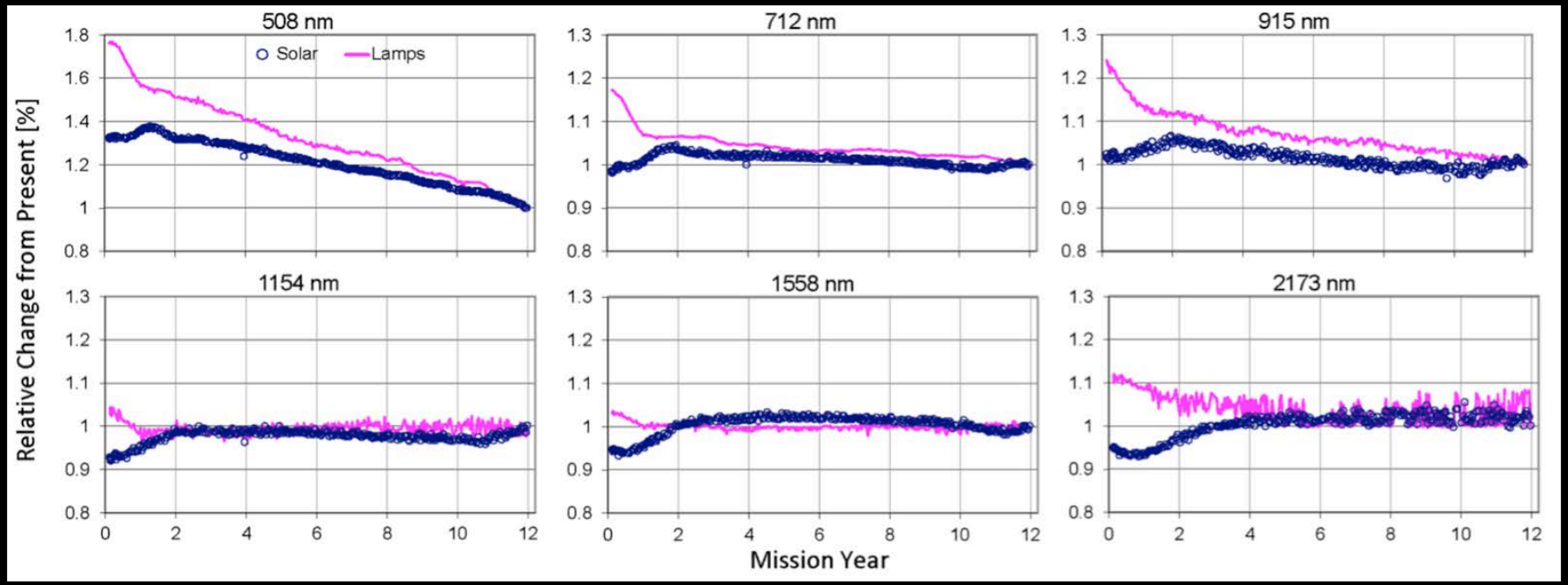

# Lunar Calibration using Hyperion

The new lunar acquisition strategy enables high quality Hyperion observations of radiometrically stable features at multiple phase angles. This new capability is realized through a significant increase in effective SNR engendered by a slow scan of the lunar surface resulting in a 32X oversampling. We continue monthly comparisons of Hyperion integrated lunar responses with the USGS Robotic Lunar Observatory (ROLO) Lunar model at near full moon to maintain the EO-1 lifetime trends.

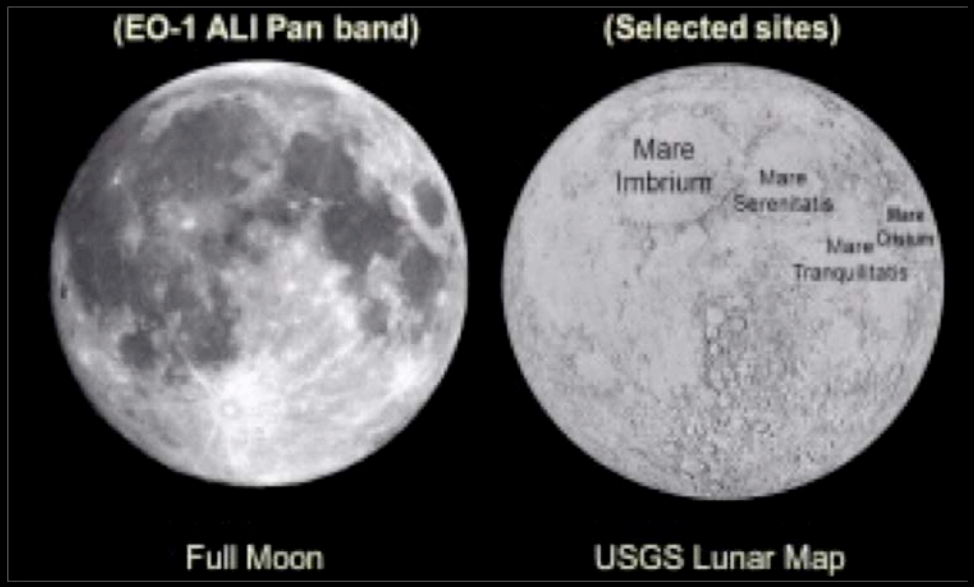


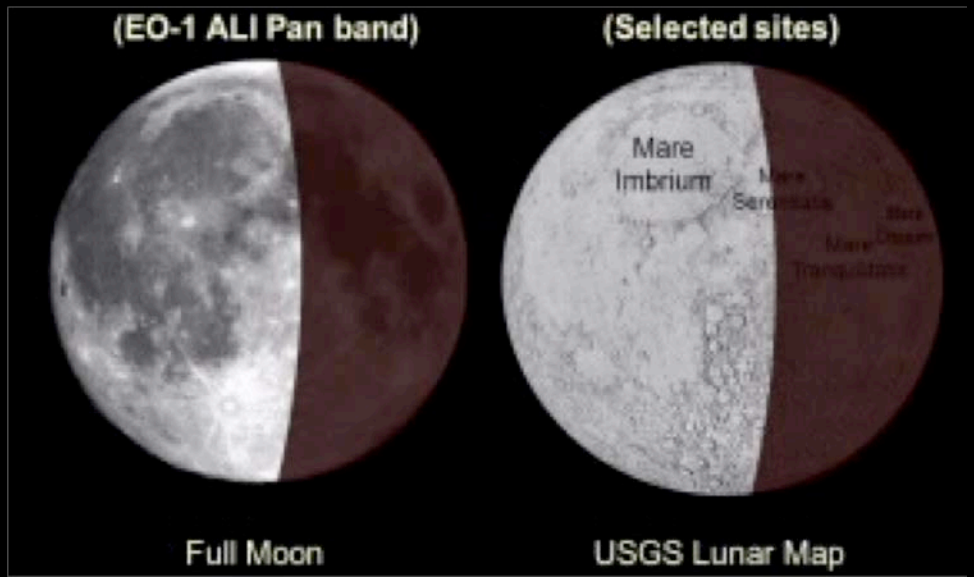

# Hyperion and the ROLO Model

- The lunar irradiances are dependent on parameters that include: the lunar librations, nutation, phase angles, viewing locations, solar distances. These factors are incorporated in the ROLO model.
- The EO-1 mission uses the ROLO model only as a basis to normalize the Hyperion data for long-term stability trending, not for absolute calibration comparison purposes.
- The Hyperion values are within the uncertainty of the ROLO comparisons with other instruments (e.g. MODIS, ASTER, MISR, LDCM) as shown by Kieffer and Stone (2005, *Astronomical Journal)* describing the ROLO model in detail. There have been on-going discussions with the model authors regarding these differences.

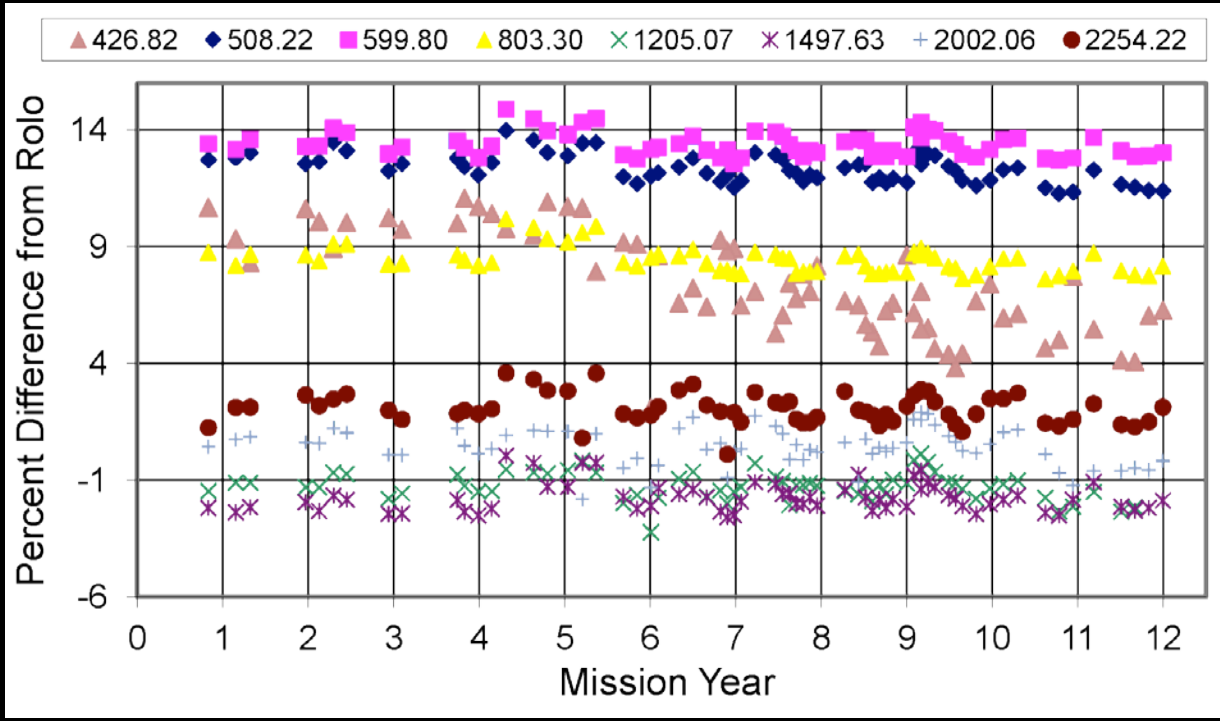


Comparison of the Hyperion integrated lunar responses with the USGS Robotic Lunar Observatory (ROLO) Lunar model.

# Trends

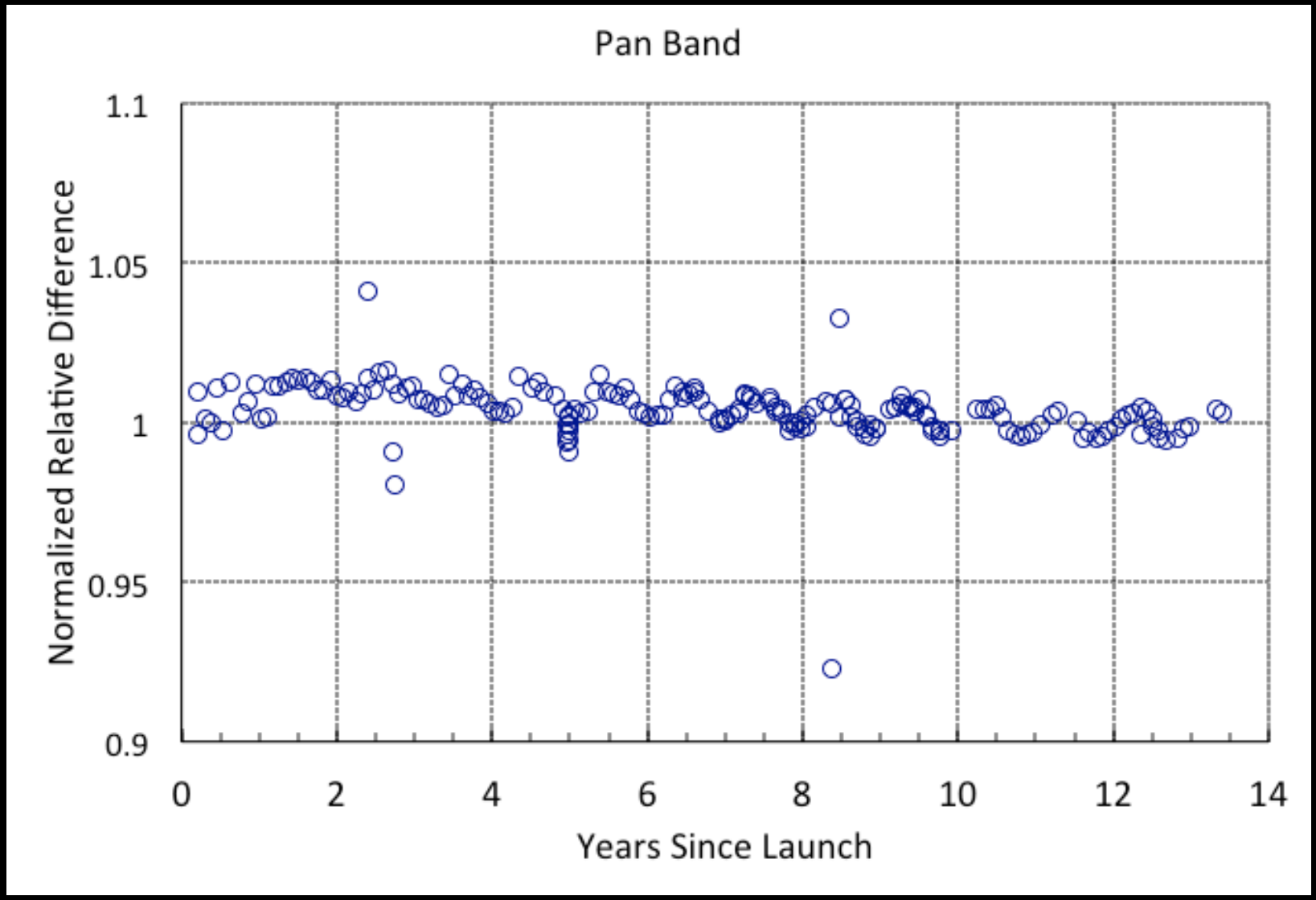
Pan Band
Normalized Relative Difference
1.1
1.05
1
0.95
0.9
0
2
4
6
8
10
12
14
Years Since Launch

# Monitoring Hyperion stability and sub-pixel heterogeneity in a pseudo-invariant desert site

## Objectives/Questions

- How stable is Hyperion through time with atmospherically corrected land surface reflectance from multiple correction approaches?
- Can Hyperion be used to cross calibrate a virtual constellation for land surface imaging?
- Can high-resolution commercial data be used to understand sub 30m pixel variability in Hyperion data?

## Study Area

- CEOS – core validation sites
  - Hyperion data has been routinely collected in the Libyan desert (Libya-4)
  - Other studies have used this site to monitor sensor degradation and cross-calibrate measurements
  - Landsat ETM+, MSS, SRTM, MODIS, EO-1

Chander et al. 2010

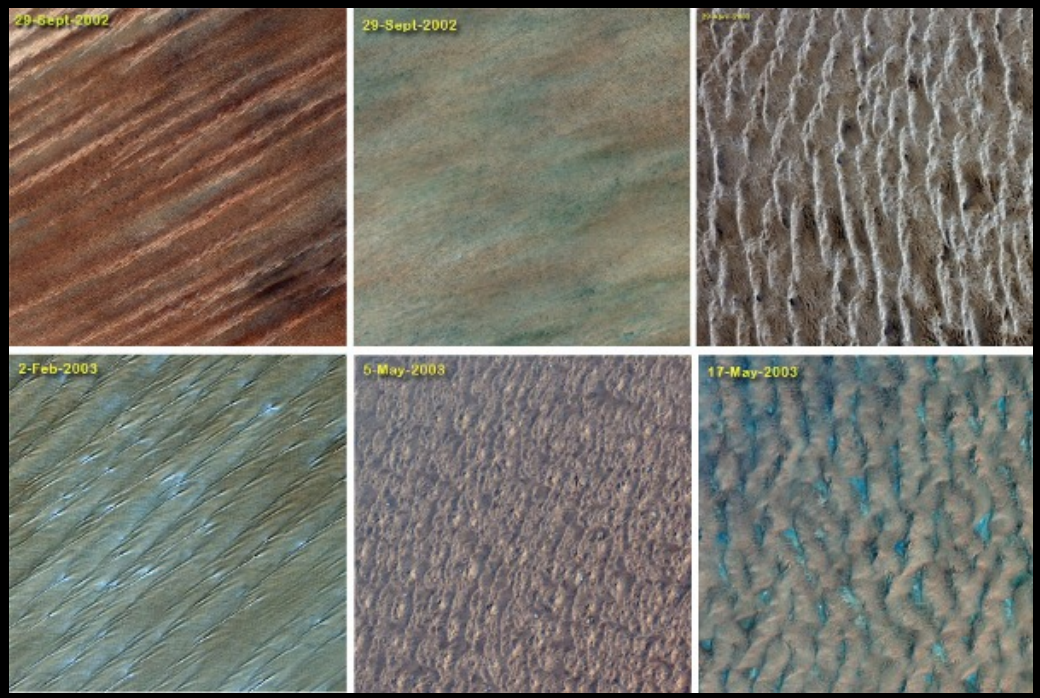


*Neigh et al. 2014*

# Hyperion Over Desert Calibration Sites

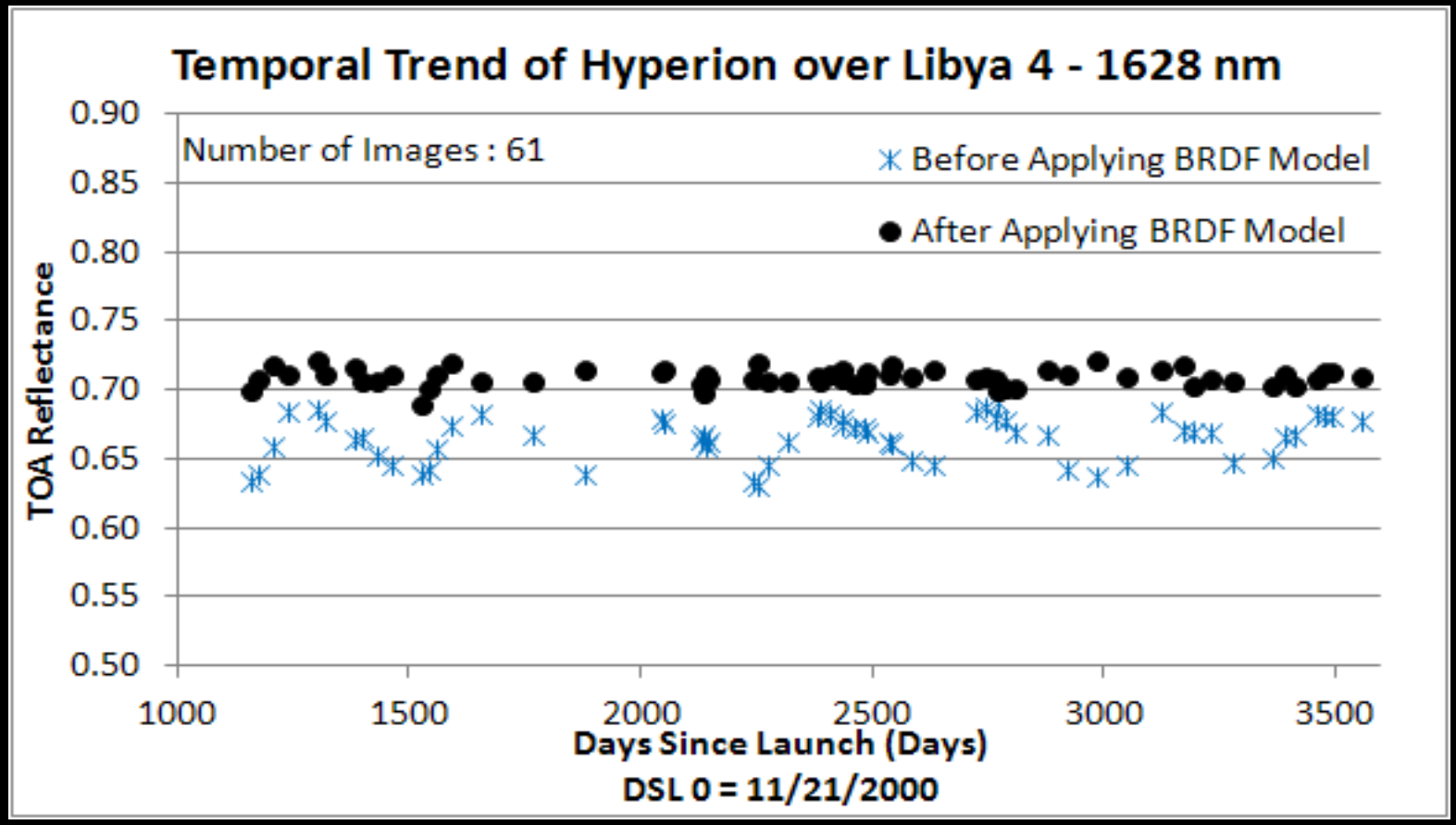


Trending for Hyperion over Libya 4 (channel 1628 nm) and RRVP (means and st.dev per band). Similar results are obtained for the other high transmittance channels as well.

# Hyperion Atmospheric Correction

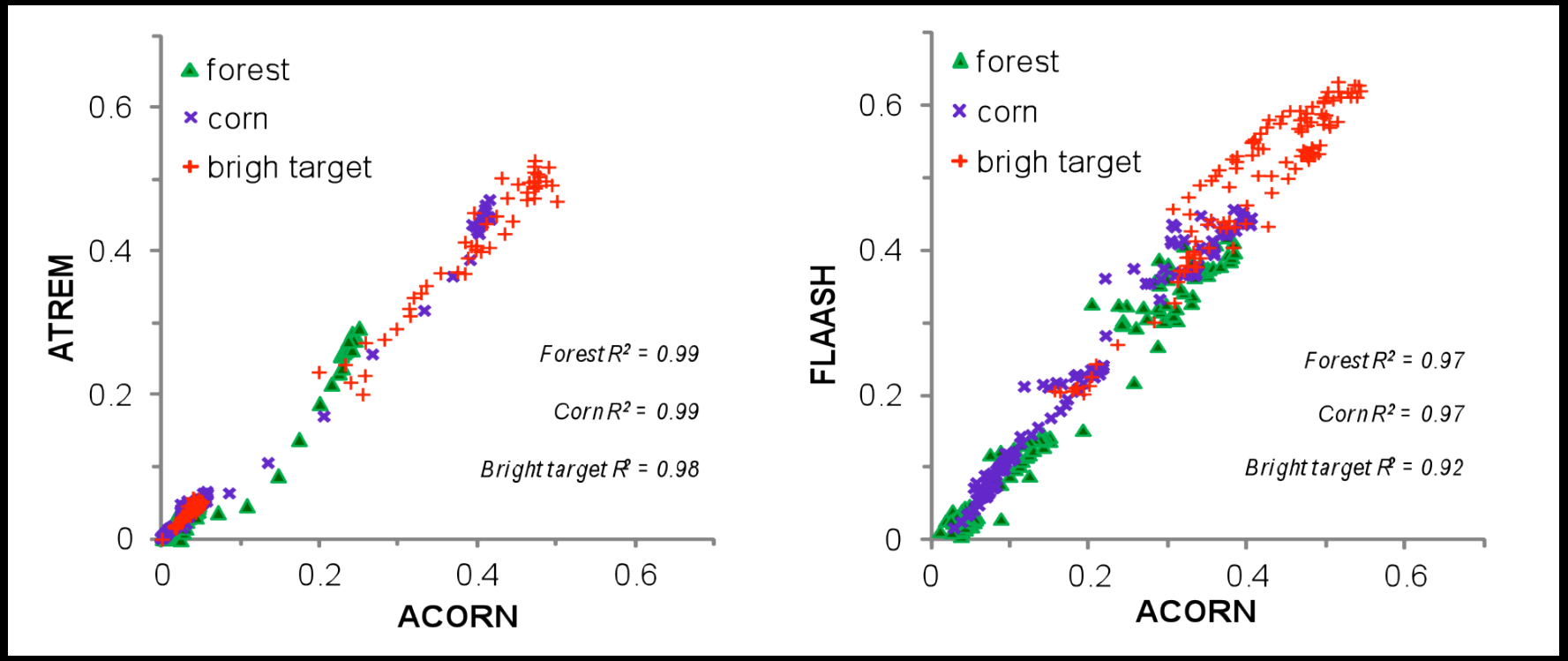


Comparison of the atmospheric correction routines ATREM [left] and FLAASH [right] (available on user demand at http://eo1.geobliki.com) versus ACORN. Different geographical areas and images were used in this comparison. However, the results are relatively similar overall ($r^2$ ~ 0.92 to 0.99), and for the same land cover types that include forest, agriculture (corn), and bright targets (e.g., sand, soil, concrete etc.). The axes indicate the relative value for reflectance (0-1).

# Duke Forest : PRI4 & *NEP*

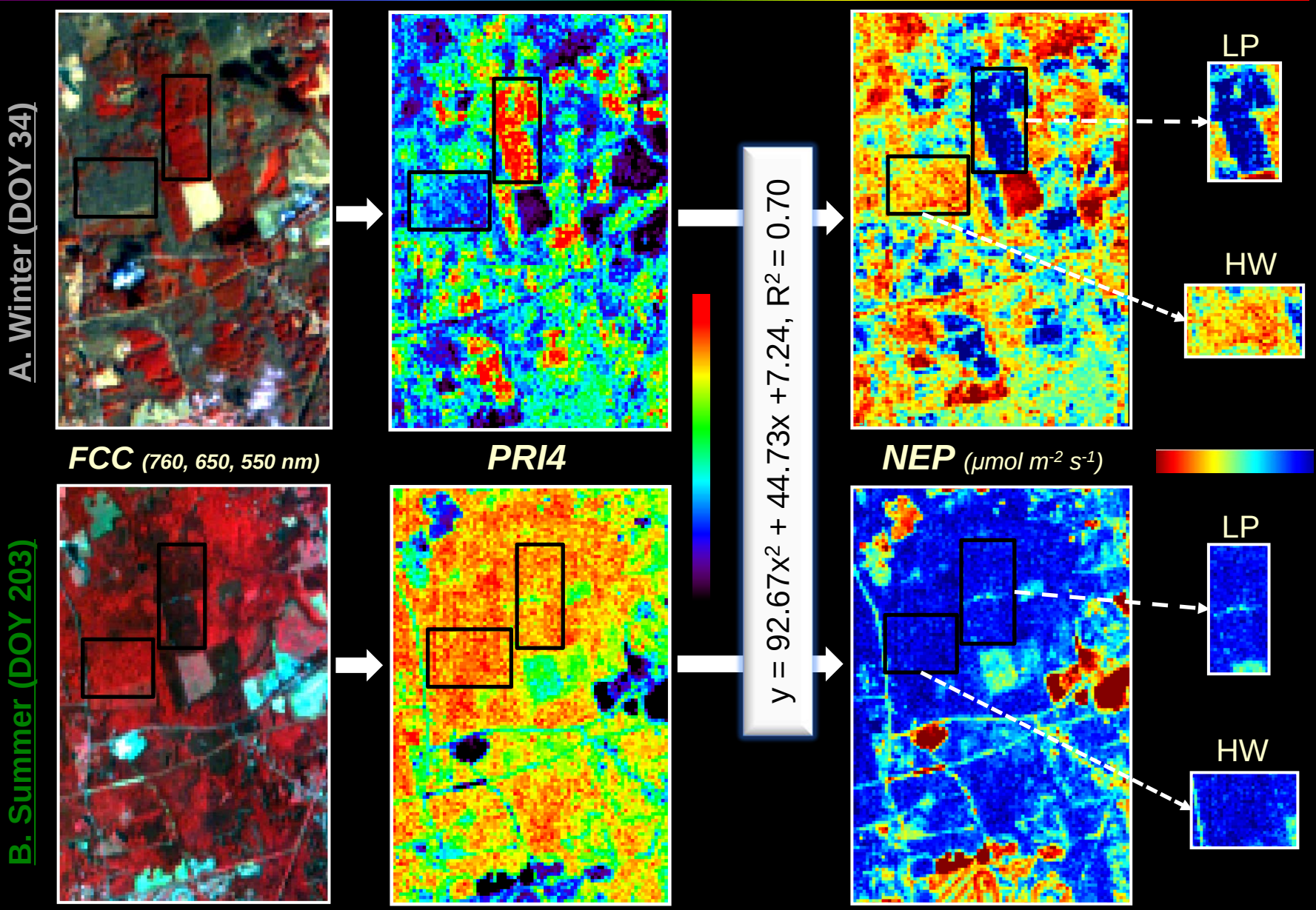

# Stepwise Linear Regression - LUE

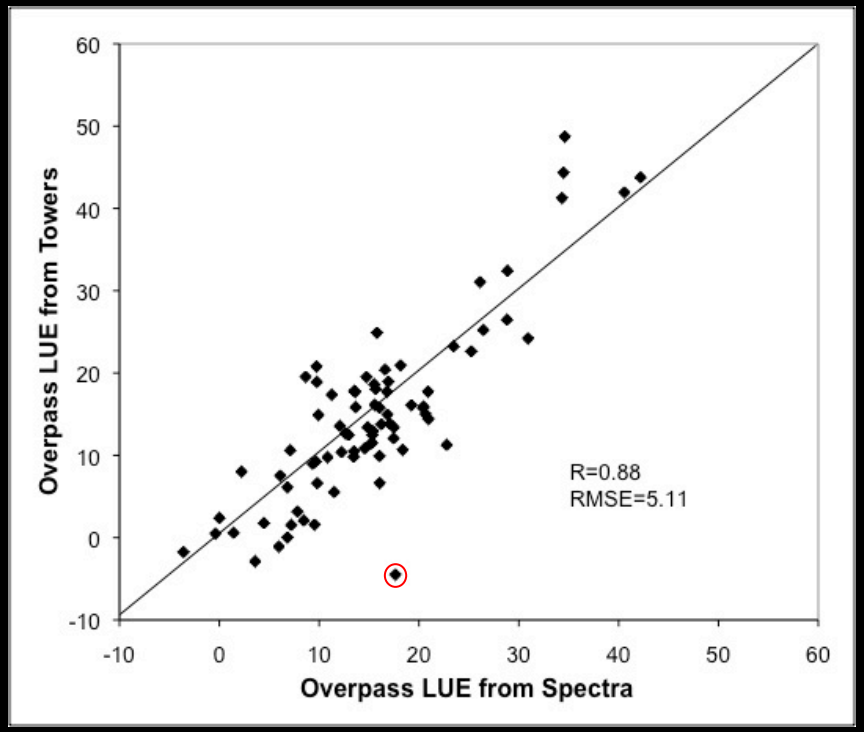


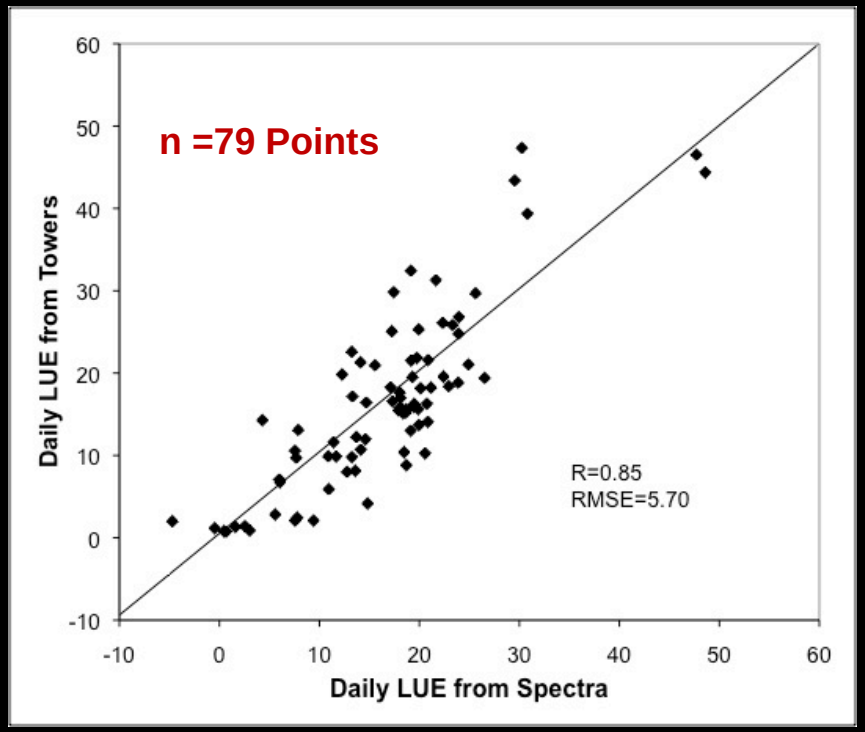


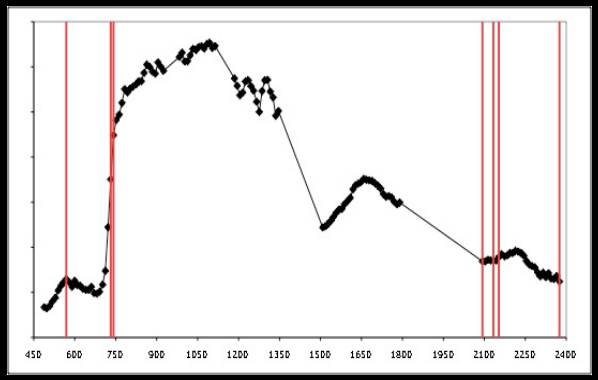

Used Bands: R569, R732, R742, R2093, R2133, R2153, R2375

* Match Hyperion imagery with flux data from LaThuile Fluxnet Synthesis

* Observations of 33 different flux tower sites (n = 80), 2001 – 2007.

* Multiple vegetation types observed during mid-growing season.

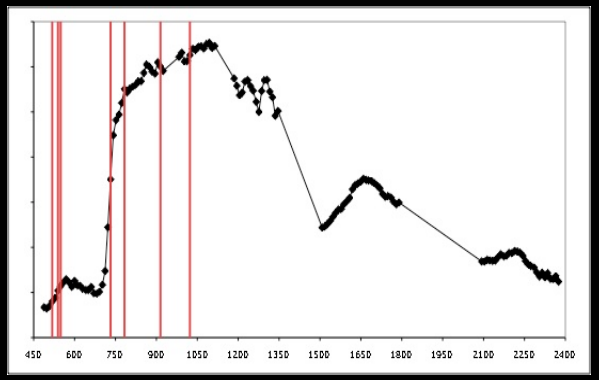

Used Bands: R518, R539, R549, R732, R783, R915, R1023

# USDA Cornfield site 2008

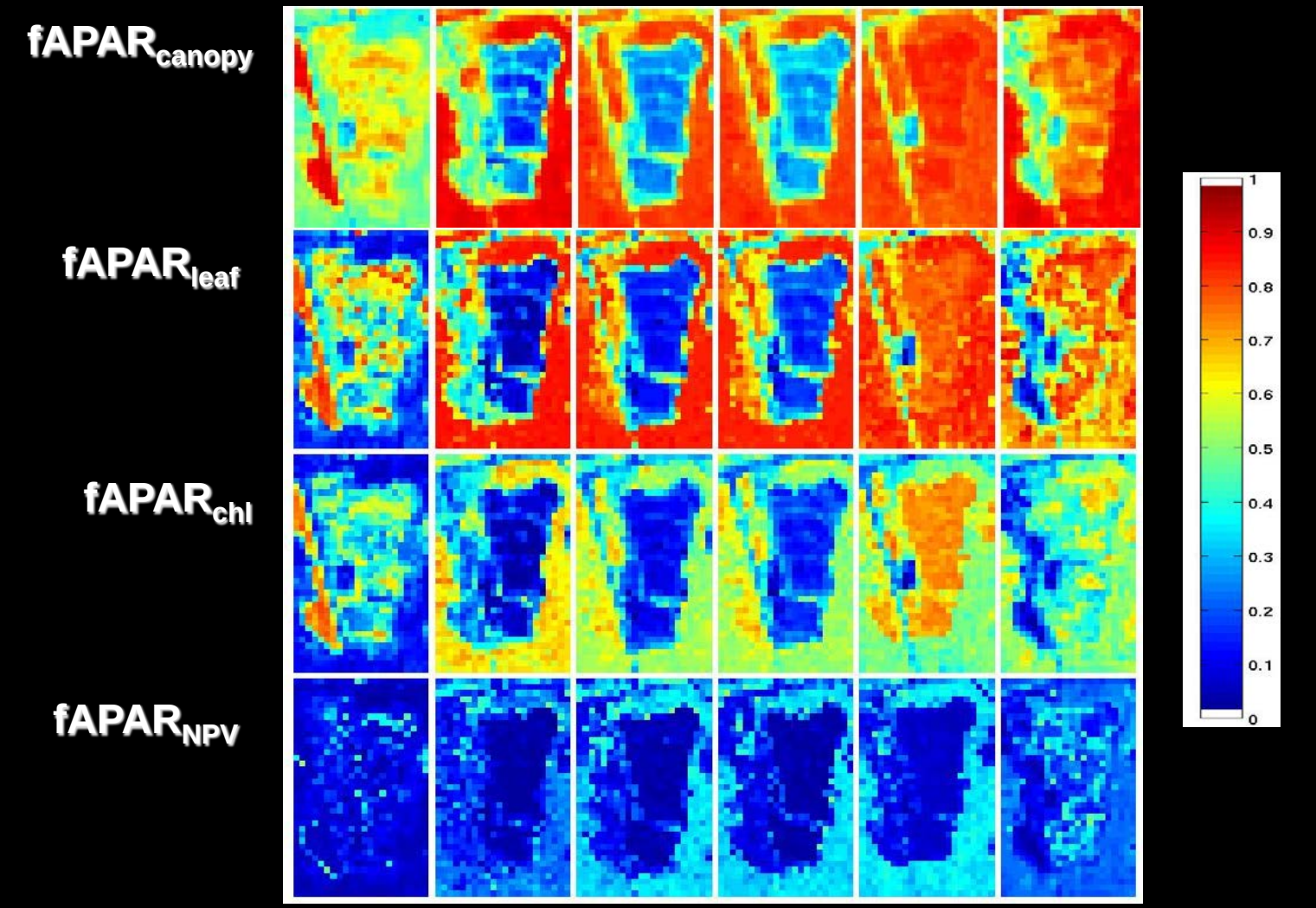

# USDA/OPE3 Corn Field

Compare LUEchl vs. PRI: Hyperion [▲] and *in situ* ASD measurements [O]

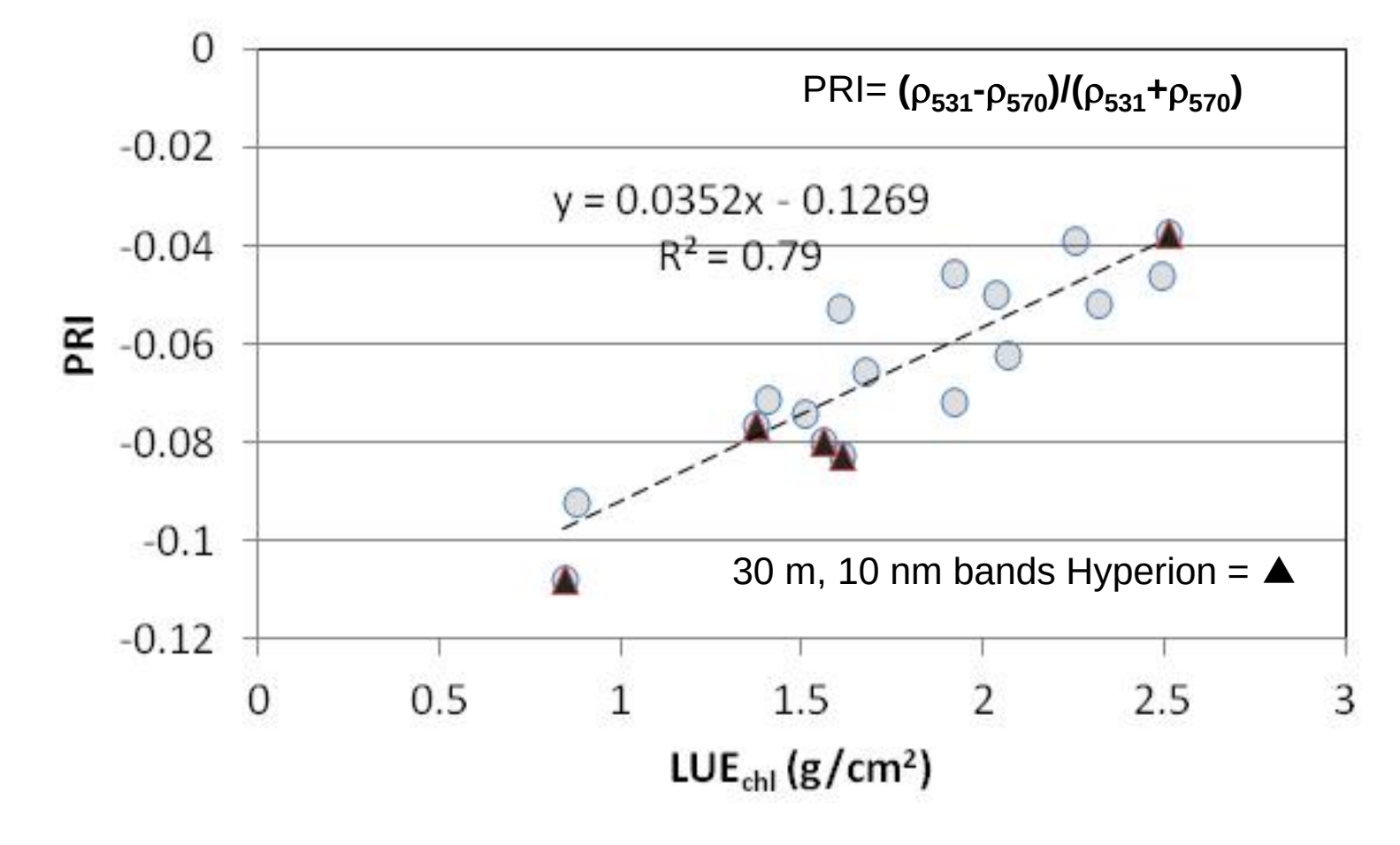


*Triangles over Circles are for the 5 days having both ASD and Hyperion images (2008 DOY 172, 190, 195, 231, 277). Hyperion data:* 30 m, 10 nm bands.

# Hyperion Data

## Frenchman Flat

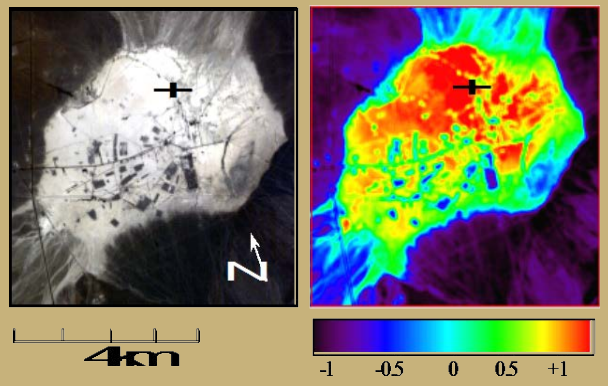


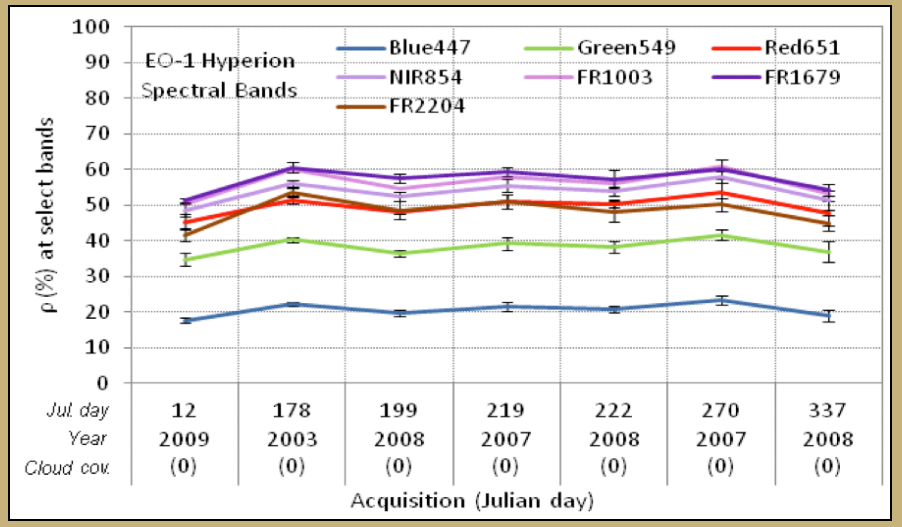


## Railroad Valley Playa

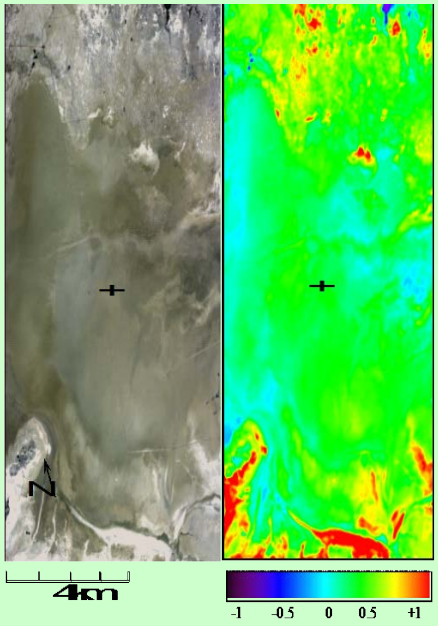


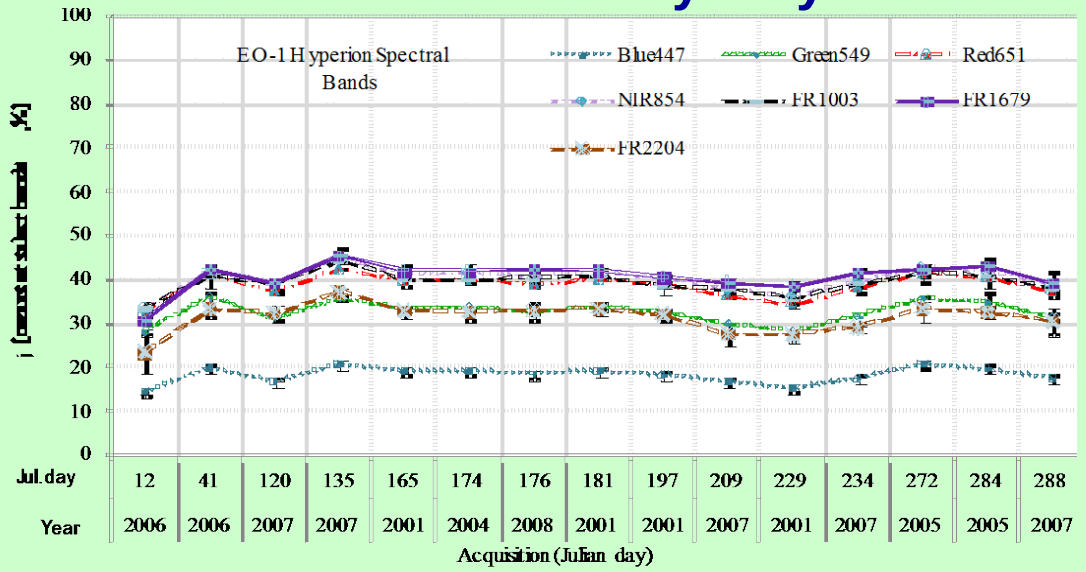

# IEEE JSTARS EO-1 Special Issue 2013

IEEE JOURNAL OF
SELECTED TOPICS IN APPLIED EARTH OBSERVATIONS AND REMOTE SENSING

A PUBLICATION OF THE IEEE GEOSCIENCE AND REMOTE SENSING SOCIETY

APRIL 2013 VOLUME 6 NUMBER 2 IJSTHZ (ISSN 1939-1404)

PART I OF THREE PARTS

SPECIAL ISSUE ON THE EARTH OBSERVING ONE (EO-1) SATELLITE MISSION: OVER A DECADE IN SPACE

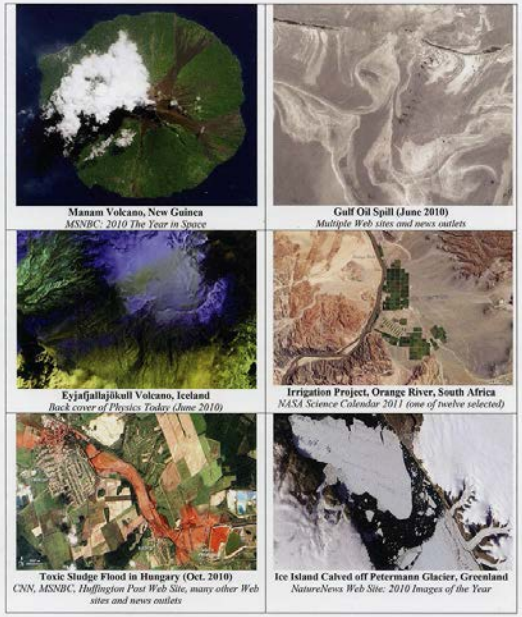

Manam Volcano, New Guinea
*MSNBC: 2010 The Year in Space*

Gulf Oil Spill (June 2010)
*Multiple Web sites and news outlets*

Eyjafjallajökull Volcano, Iceland
*Back cover of Physics Today (June 2010)*

Irrigation Project, Orange River, South Africa
*NASA Science Calendar 2011 (one of twelve selected)*

Toxic Sludge Flood in Hungary (Oct. 2010)
*CNN, MSNBC, Huffington Post Web Site, many other Web sites and news outlets*

Ice Island Calved off Petermann Glacier, Greenland
*NatureNews Web Site: 2010 Images of the Year*

Examples of ALI images posted by NASA's Earth Observatory. (See Middleton *et al.*, pp. 243–256.)

# Hyperion: Guánica Dry Forest in Puerto Rico

Forest vegetation class abundances tracked seasonal changes in rainfall – decreasing from February to March, increasing from April to May, and decreasing from June to August.

These changes are shown in NDVI and abundance maps for endmember classes: forest vegetation, mangroves, rocky outcrops, crops (vegetation), crops (soil), and buildings.

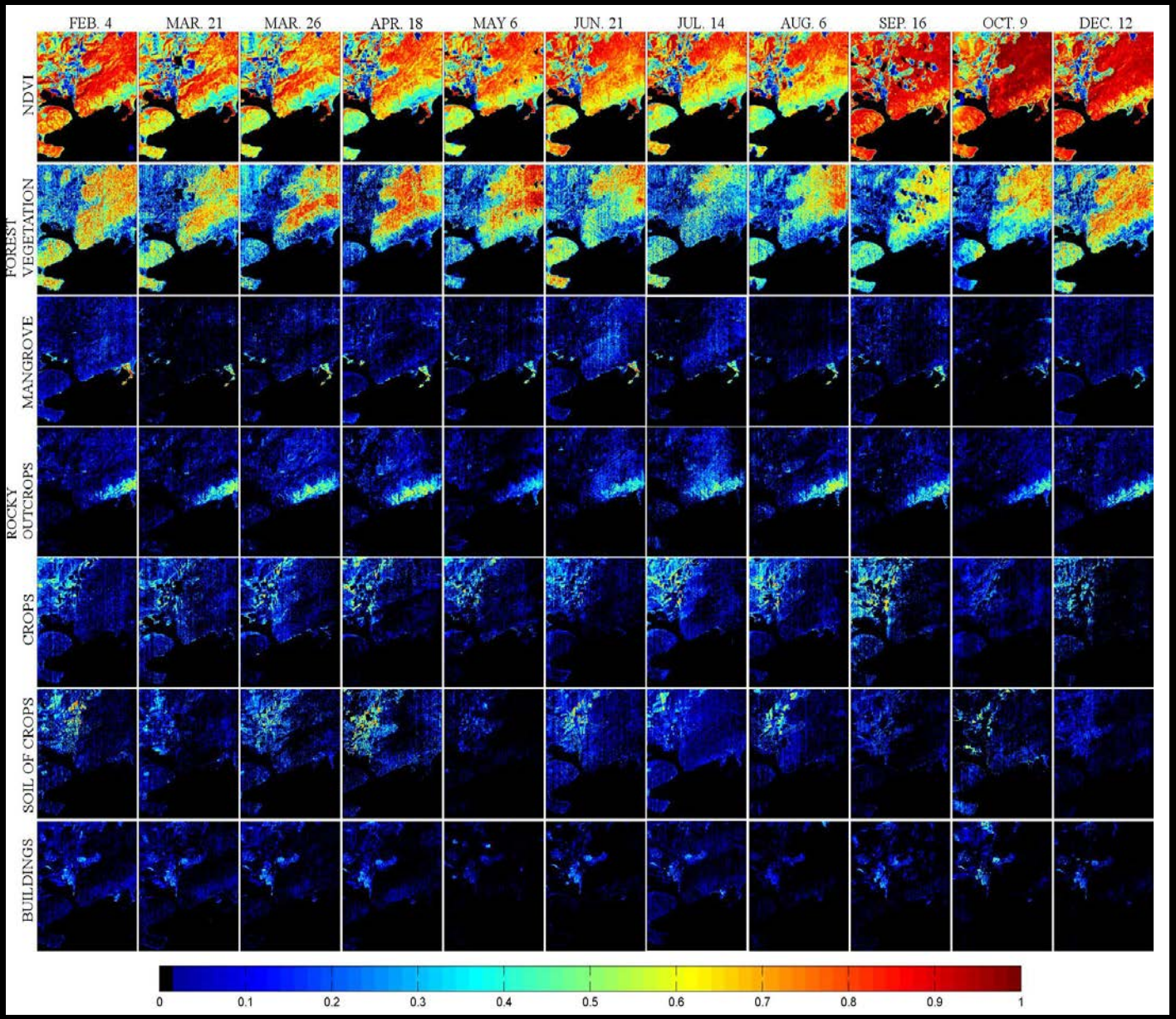


M. Goenaga *et al.*
*JSTARS 2013*

# Hyperion in Peruvian Forests

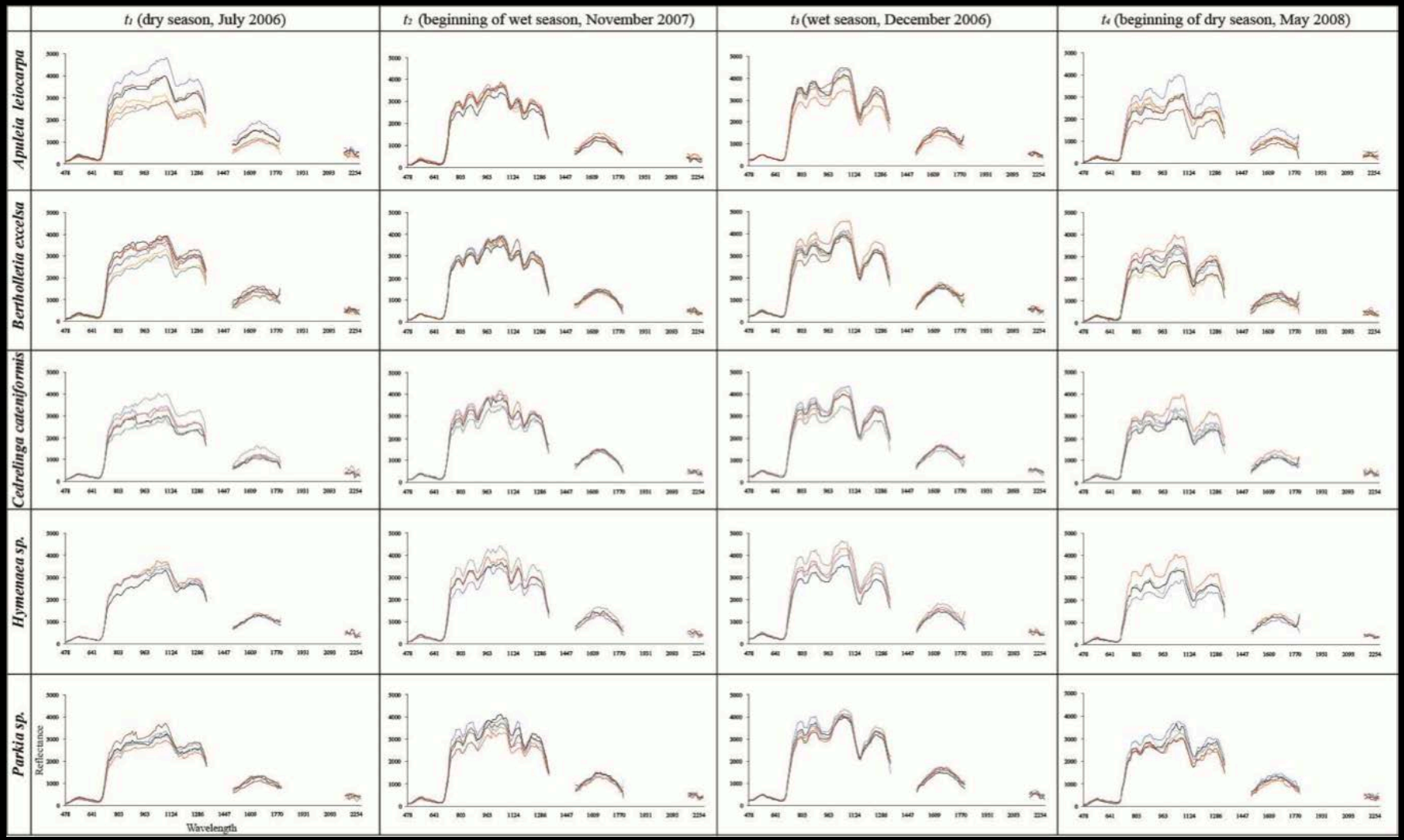


Spectra of tree crowns of the 5 Peruvian tree taxa studied (screened dataset shown only) at the 4 times examined (t1 - t4), with uncalibrated Hyperion bands removed; colors represent different individuals of the same taxon. Apparent reflectance values were scaled from floating point into integer values using a 10,000 scale factor.

M. Papes et al., JSTARS 2013

# Hyperion - Reflectance, Functional Type Cover, and LUE

Day 201, 2009, Image subset around Barrow, AK
Field measurements scaled to region find a 5-fold variation in LUE

R = Reflectance at 834 nm
G = Reflectance at 671 nm
B = Reflectance at 549 nm

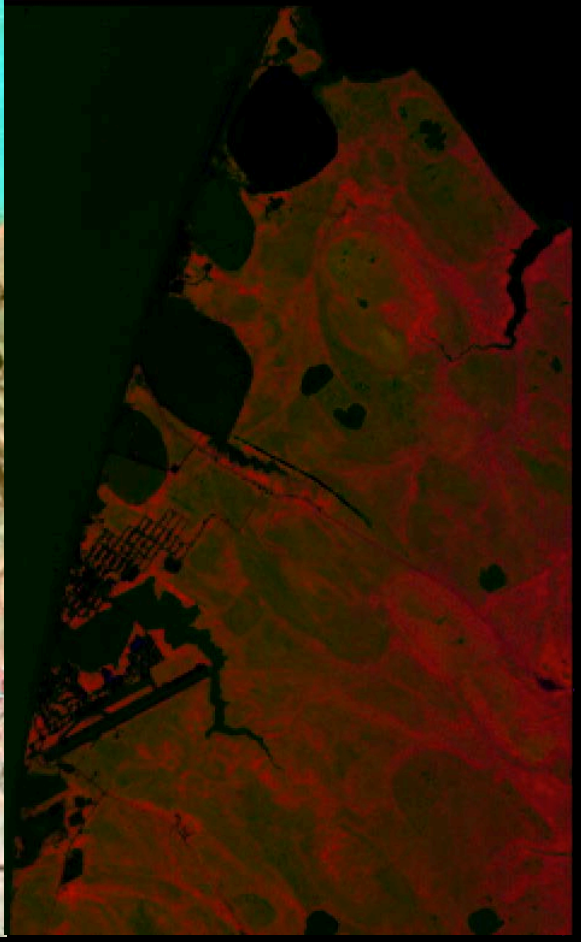

R = Vascular Plant Cover
G = Moss Cover
B = Lichen Cover
Scale from 0 – 100%

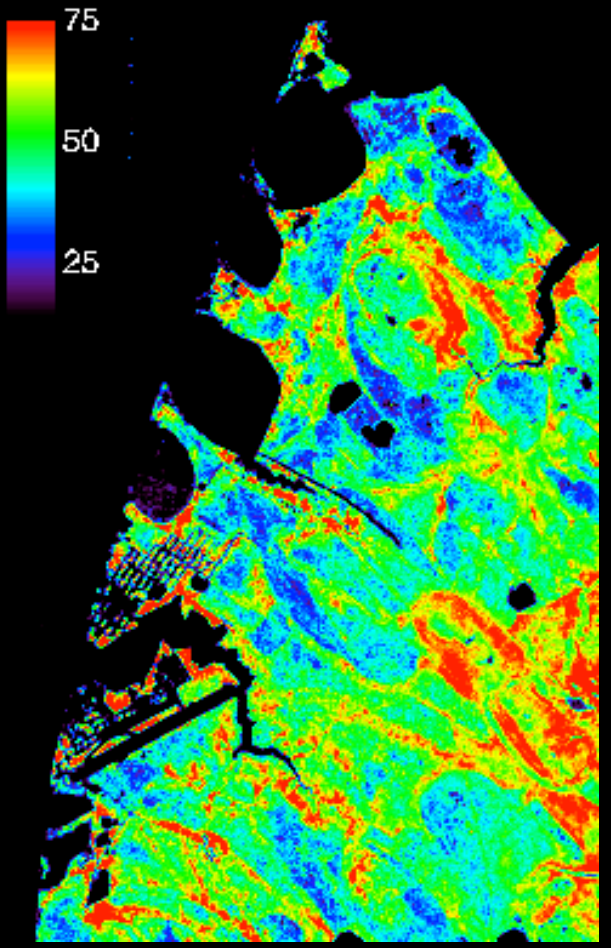


Light Use Efficiency
(x10,000)
Based on coverage

# Hyperion in Australia (Darwin)

*M. Hill et al.*
*JSTARS 2013*

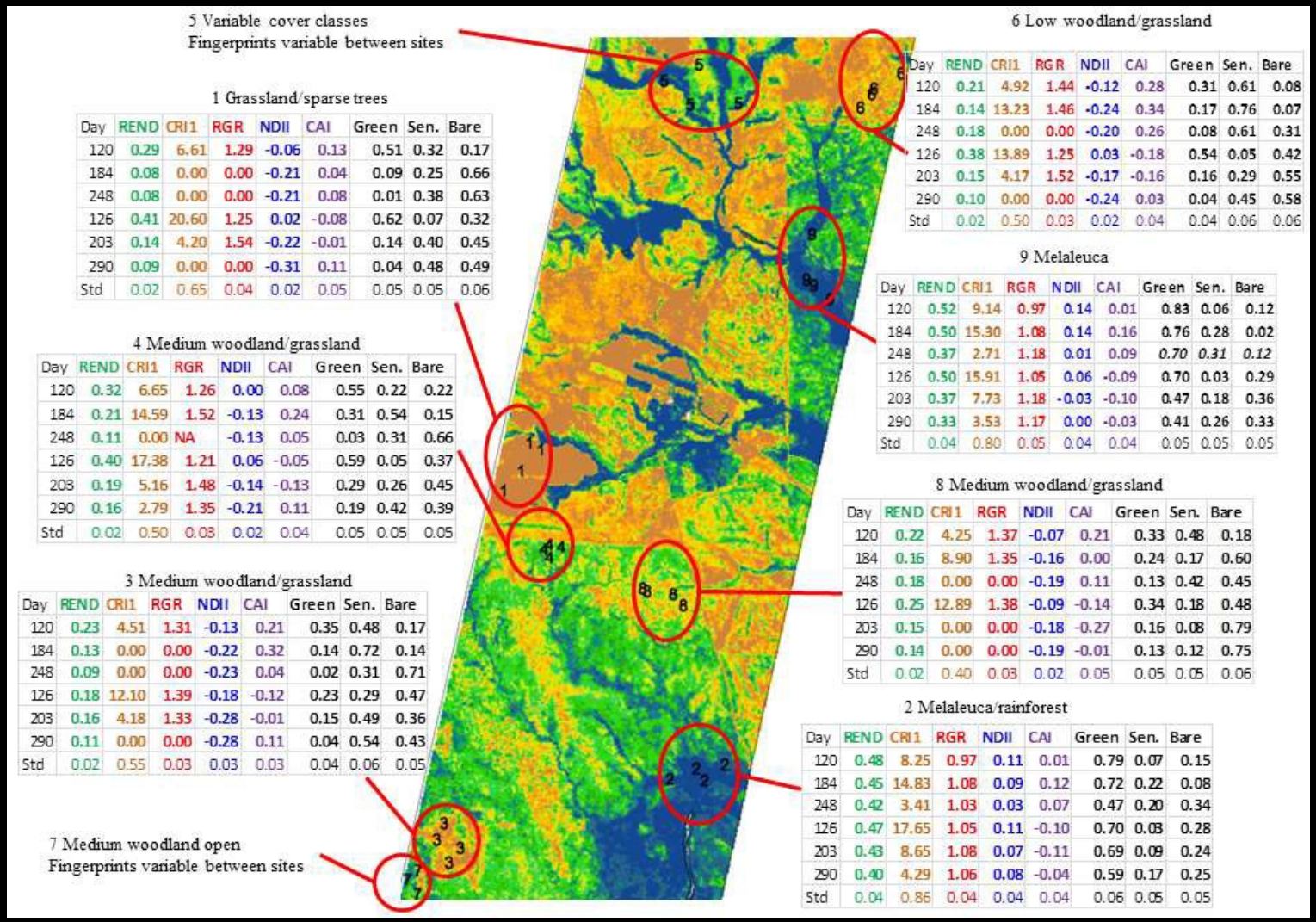


1 Grassland/sparse trees

| Day | REND | CRI1 | RGR | NDII | CAI | Green | Sen. | Bare |
|---|---|---|---|---|---|---|---|---|
| 120 | 0.29 | 6.61 | 1.29 | -0.06 | 0.13 | 0.51 | 0.32 | 0.17 |
| 184 | 0.08 | 0.00 | 0.00 | -0.21 | 0.04 | 0.09 | 0.25 | 0.66 |
| 248 | 0.08 | 0.00 | 0.00 | -0.21 | 0.08 | 0.01 | 0.38 | 0.63 |
| 126 | 0.41 | 20.60 | 1.25 | 0.02 | -0.08 | 0.62 | 0.07 | 0.32 |
| 203 | 0.14 | 4.20 | 1.54 | -0.22 | -0.01 | 0.14 | 0.40 | 0.45 |
| 290 | 0.09 | 0.00 | 0.00 | -0.31 | 0.11 | 0.04 | 0.48 | 0.49 |
| Std | 0.02 | 0.65 | 0.04 | 0.02 | 0.05 | 0.05 | 0.05 | 0.06 |

4 Medium woodland/grassland

| Day | REND | CRI1 | RGR | NDII | CAI | Green | Sen. | Bare |
|---|---|---|---|---|---|---|---|---|
| 120 | 0.32 | 6.65 | 1.26 | 0.00 | 0.08 | 0.55 | 0.22 | 0.22 |
| 184 | 0.21 | 14.59 | 1.52 | -0.13 | 0.24 | 0.31 | 0.54 | 0.15 |
| 248 | 0.11 | 0.00 | NA | -0.13 | 0.05 | 0.03 | 0.31 | 0.66 |
| 126 | 0.40 | 17.38 | 1.21 | 0.06 | -0.05 | 0.59 | 0.05 | 0.37 |
| 203 | 0.19 | 5.16 | 1.48 | -0.14 | -0.13 | 0.29 | 0.26 | 0.45 |
| 290 | 0.16 | 2.79 | 1.35 | -0.21 | 0.11 | 0.19 | 0.42 | 0.39 |
| Std | 0.02 | 0.50 | 0.03 | 0.02 | 0.04 | 0.05 | 0.05 | 0.05 |

3 Medium woodland/grassland

| Day | REND | CRI1 | RGR | NDII | CAI | Green | Sen. | Bare |
|---|---|---|---|---|---|---|---|---|
| 120 | 0.23 | 4.51 | 1.31 | -0.13 | 0.21 | 0.35 | 0.48 | 0.17 |
| 184 | 0.13 | 0.00 | 0.00 | -0.22 | 0.32 | 0.14 | 0.72 | 0.14 |
| 248 | 0.09 | 0.00 | 0.00 | -0.23 | 0.04 | 0.02 | 0.31 | 0.71 |
| 126 | 0.18 | 12.10 | 1.39 | -0.18 | -0.12 | 0.23 | 0.29 | 0.47 |
| 203 | 0.16 | 4.18 | 1.33 | -0.28 | -0.01 | 0.15 | 0.49 | 0.36 |
| 290 | 0.11 | 0.00 | 0.00 | -0.28 | 0.11 | 0.04 | 0.54 | 0.43 |
| Std | 0.02 | 0.55 | 0.03 | 0.03 | 0.03 | 0.04 | 0.06 | 0.05 |

6 Low woodland/grassland

| Day | REND | CRI1 | RGR | NDII | CAI | Green | Sen. | Bare |
|---|---|---|---|---|---|---|---|---|
| 120 | 0.21 | 4.92 | 1.44 | -0.12 | 0.28 | 0.31 | 0.61 | 0.08 |
| 184 | 0.14 | 13.23 | 1.46 | -0.24 | 0.34 | 0.17 | 0.76 | 0.07 |
| 248 | 0.18 | 0.00 | 0.00 | -0.20 | 0.26 | 0.08 | 0.61 | 0.31 |
| 126 | 0.38 | 13.89 | 1.25 | 0.03 | -0.18 | 0.54 | 0.05 | 0.42 |
| 203 | 0.15 | 4.17 | 1.52 | -0.17 | -0.16 | 0.16 | 0.29 | 0.55 |
| 290 | 0.10 | 0.00 | 0.00 | -0.24 | 0.03 | 0.04 | 0.45 | 0.58 |
| Std | 0.02 | 0.50 | 0.03 | 0.02 | 0.04 | 0.04 | 0.06 | 0.06 |

9 Melaleuca

| Day | REND | CRI1 | RGR | NDII | CAI | Green | Sen. | Bare |
|---|---|---|---|---|---|---|---|---|
| 120 | 0.52 | 9.14 | 0.97 | 0.14 | 0.01 | 0.83 | 0.06 | 0.12 |
| 184 | 0.50 | 15.30 | 1.08 | 0.14 | 0.16 | 0.76 | 0.28 | 0.02 |
| 248 | 0.37 | 2.71 | 1.18 | 0.01 | 0.09 | *0.70* | *0.31* | *0.12* |
| 126 | 0.50 | 15.91 | 1.05 | 0.06 | -0.09 | 0.70 | 0.03 | 0.29 |
| 203 | 0.37 | 7.73 | 1.18 | -0.03 | -0.10 | 0.47 | 0.18 | 0.36 |
| 290 | 0.33 | 3.53 | 1.17 | 0.00 | -0.03 | 0.41 | 0.26 | 0.33 |
| Std | 0.04 | 0.80 | 0.05 | 0.04 | 0.04 | 0.05 | 0.05 | 0.05 |

8 Medium woodland/grassland

| Day | REND | CRI1 | RGR | NDII | CAI | Green | Sen. | Bare |
|---|---|---|---|---|---|---|---|---|
| 120 | 0.22 | 4.25 | 1.37 | -0.07 | 0.21 | 0.33 | 0.48 | 0.18 |
| 184 | 0.16 | 8.90 | 1.35 | -0.16 | 0.00 | 0.24 | 0.17 | 0.60 |
| 248 | 0.18 | 0.00 | 0.00 | -0.19 | 0.11 | 0.13 | 0.42 | 0.45 |
| 126 | 0.25 | 12.89 | 1.38 | -0.09 | -0.14 | 0.34 | 0.18 | 0.48 |
| 203 | 0.15 | 0.00 | 0.00 | -0.18 | -0.27 | 0.16 | 0.08 | 0.79 |
| 290 | 0.14 | 0.00 | 0.00 | -0.19 | -0.01 | 0.13 | 0.12 | 0.75 |
| Std | 0.02 | 0.40 | 0.03 | 0.02 | 0.05 | 0.05 | 0.05 | 0.06 |

2 Melaleuca/rainforest

| Day | REND | CRI1 | RGR | NDII | CAI | Green | Sen. | Bare |
|---|---|---|---|---|---|---|---|---|
| 120 | 0.48 | 8.25 | 0.97 | 0.11 | 0.01 | 0.79 | 0.07 | 0.15 |
| 184 | 0.45 | 14.83 | 1.08 | 0.09 | 0.12 | 0.72 | 0.22 | 0.08 |
| 248 | 0.42 | 3.41 | 1.03 | 0.03 | 0.07 | 0.47 | 0.20 | 0.34 |
| 126 | 0.47 | 17.65 | 1.05 | 0.11 | -0.10 | 0.70 | 0.03 | 0.28 |
| 203 | 0.43 | 8.65 | 1.08 | 0.07 | -0.11 | 0.69 | 0.09 | 0.24 |
| 290 | 0.40 | 4.29 | 1.06 | 0.08 | -0.04 | 0.59 | 0.17 | 0.25 |
| Std | 0.04 | 0.86 | 0.04 | 0.04 | 0.04 | 0.06 | 0.05 | 0.05 |

Characterization of vegetation states with vegetation index fingerprints for selected areas within land cover types for region 2 where natural savanna vegetation and grazing land use predominate. Fingerprints are shown as tables with day of year for 2005 and 2006 shown in the first column. Fractional cover values in the last three columns are in decimal proportions. Values represent the average for the sites shown. The last row shows the average standard deviation over the six image dates.

# EO-1: End of Mission

- As EO-1 continues to drift, the equatorial overpass time gets earlier and earlier,
- Equatorial image data are always usable, even in 2016. And even then, higher-latitude image data could still be acquired in the summer months.
- **The seasonal change in SZA is much larger than the change due to EO-1's orbital decay.**

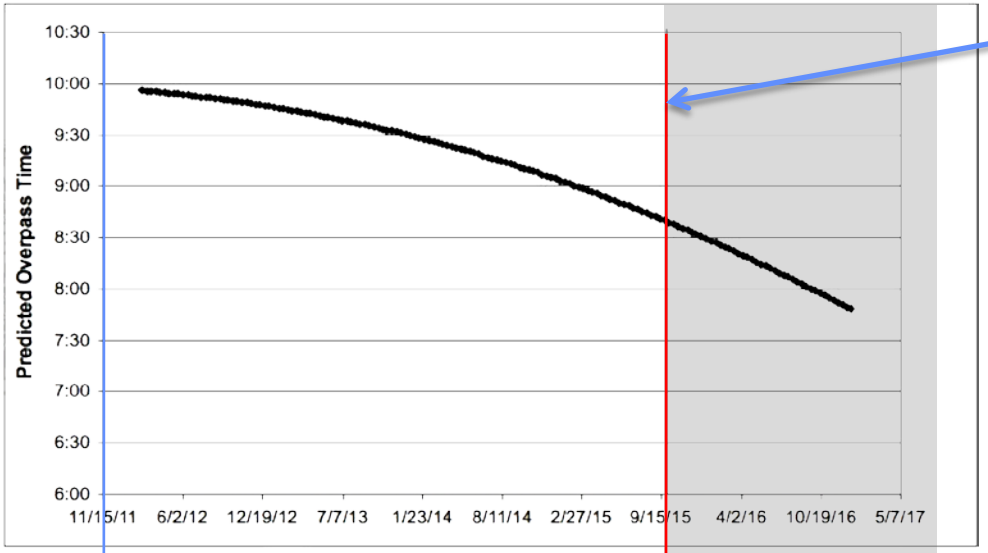


Scheduled EO-1 Shutoff Date in September 2015.

Due to the collision avoidance burn on May 9, 2014, EO-1 will be 3 minutes earlier by September 2015.

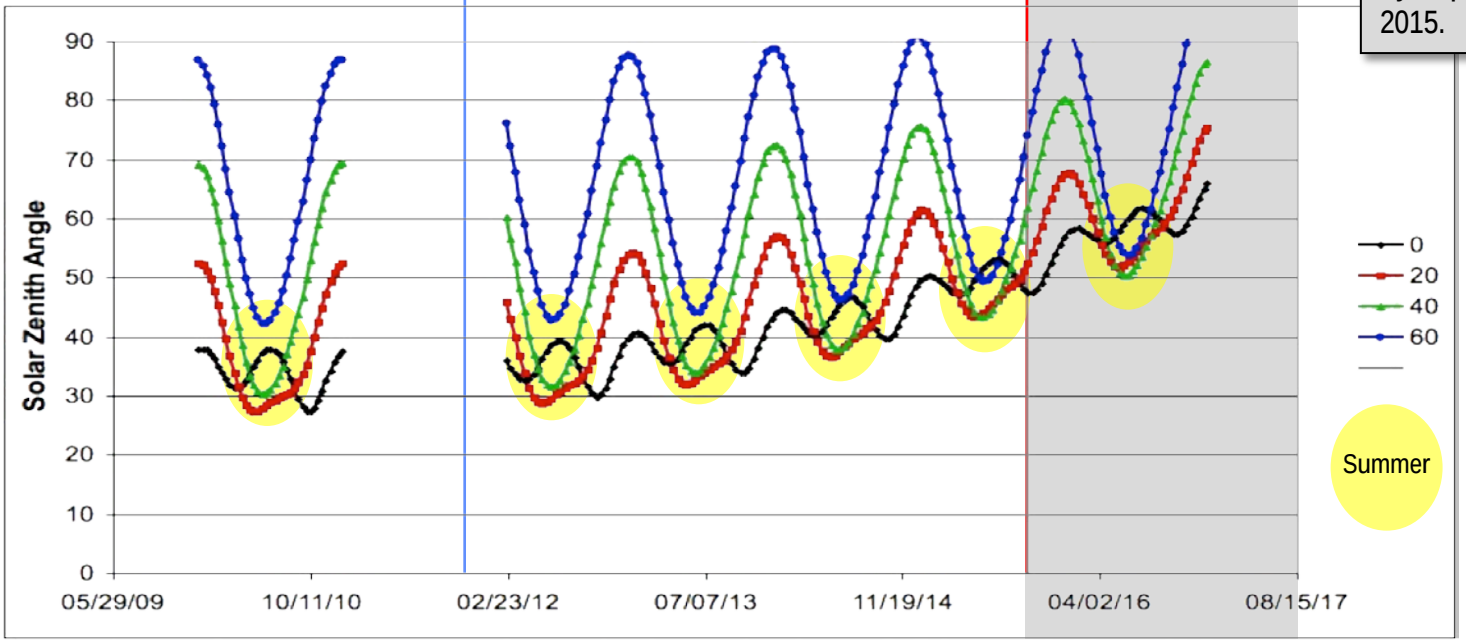

# EO-1 10th Anniversary Celebration

**December 1, 2010**

**THANK YOU!**


**Sponsored by:**
***NASA, ATK, NGC, Sigma Space, and SGT***

**NASA Goddard Space Flight Center Visitor Center**

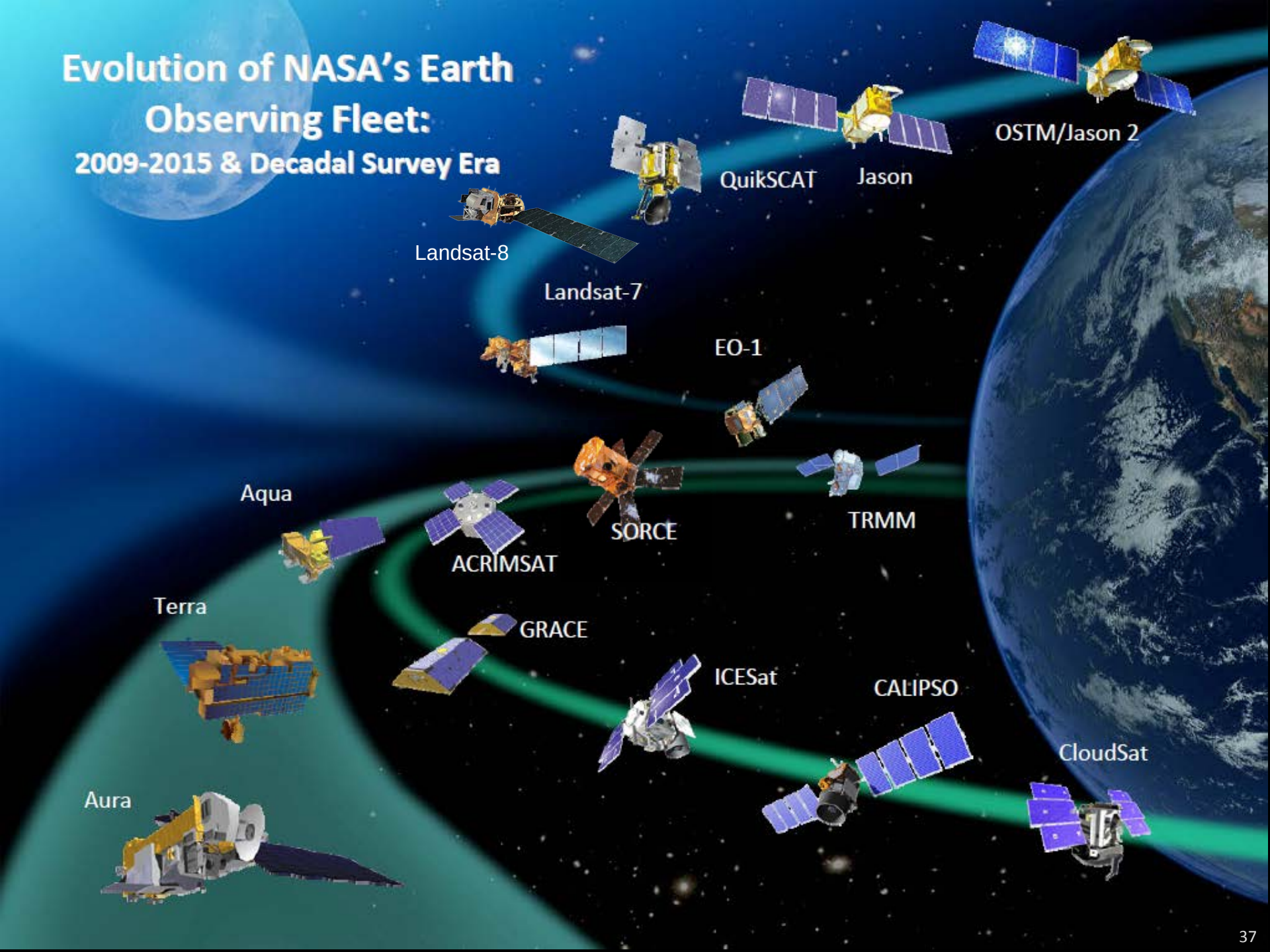
Evolution of NASA's Earth Observing Fleet:
2009-2015 & Decadal Survey Era
QuikSCAT
Jason
OSTM/Jason 2
Landsat-8
Landsat-7
EO-1
Aqua
ACRIMSAT
SORCE
TRMM
Terra
GRACE
ICESat
CALIPSO
CloudSat
Aura

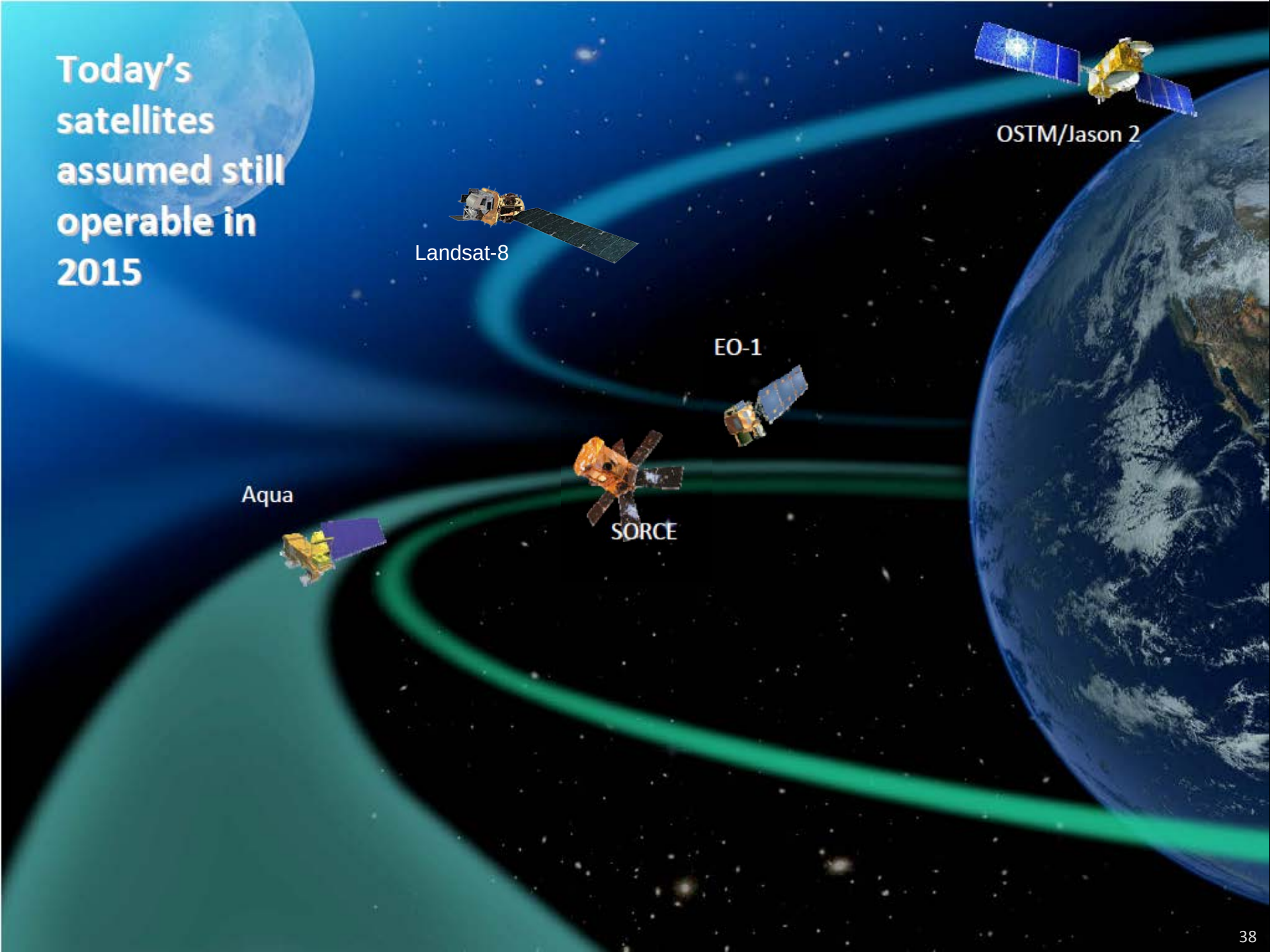
Today's satellites assumed still operable in 2015
OSTM/Jason 2
Landsat-8
EO-1
SORCE
Aqua

**Web Sites to check out:**

http://earthobservatory.nasa.gov/

http://eo1.usgs.gov/

http://eo1.gsfc.nasa.gov/

http://eros.usgs.gov/imagegallery/

http://landsat.usgs.gov/

# Applications for Hyperion

## Applications

- Mineral Mapping
- Hot Targets: Fires, Volcanoes
- Vegetation: Forests, Agriculture
- Canopy Water & Surface Water

# Species Recognition

Landsat 7 Hyperion AVIRIS

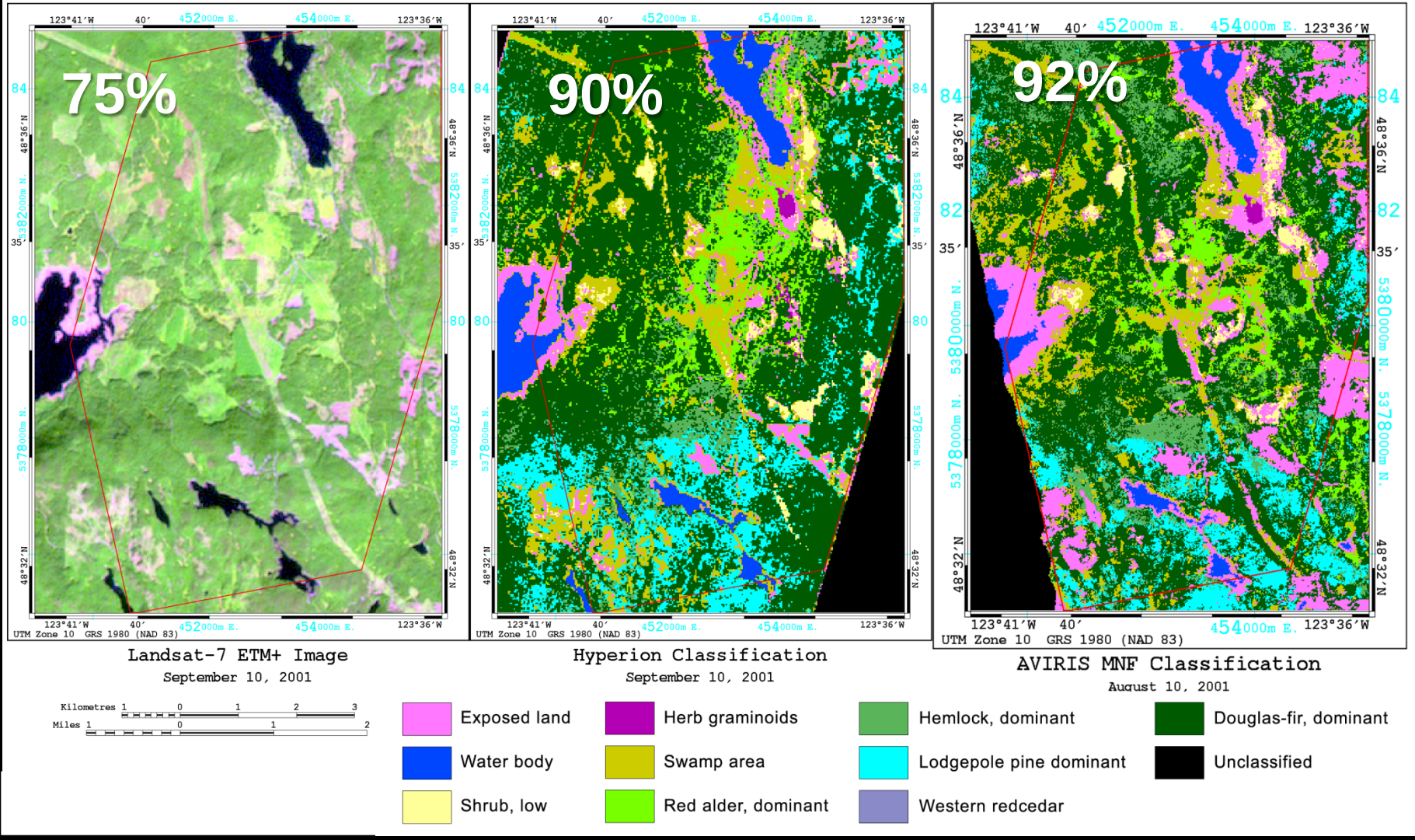

# Hyperion Maps Minerals

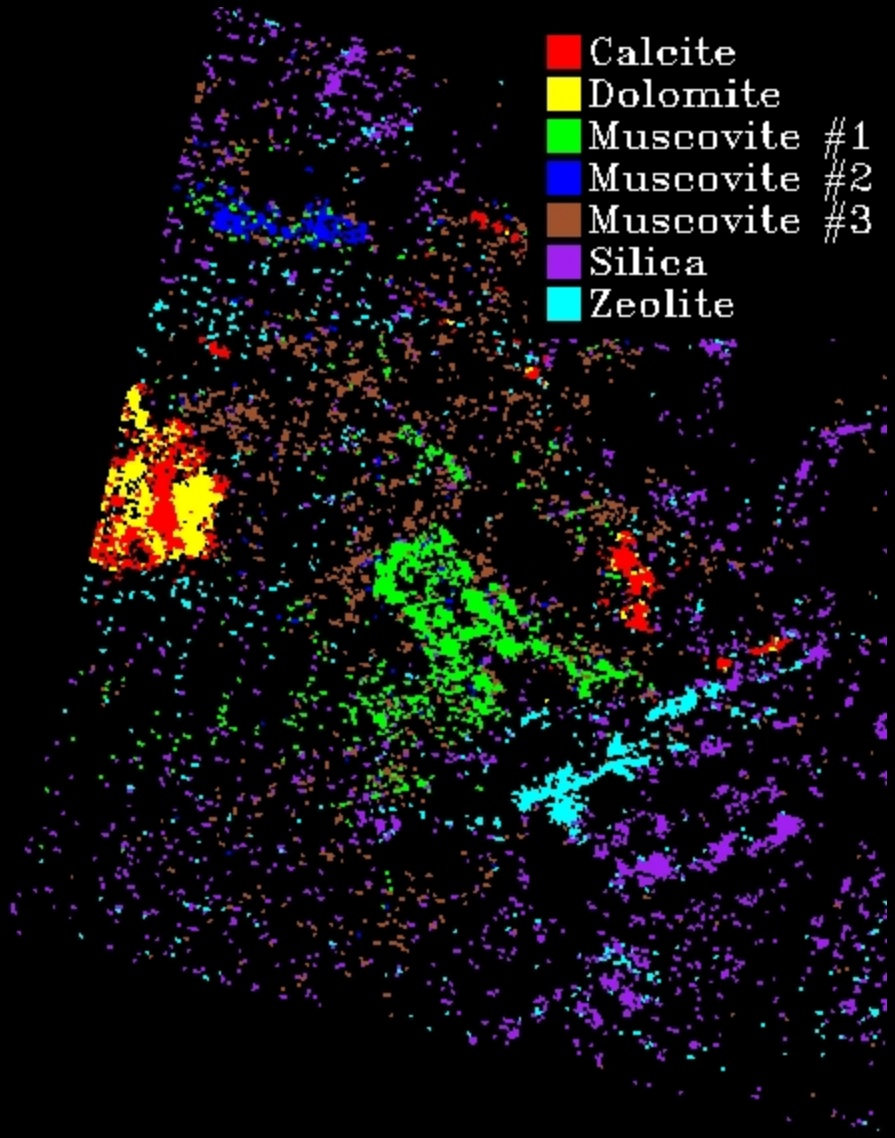


An example of Hyperion's mineral mapping capability relying on full spectrum hyperspectral imaging from 0.4 to 2.45 μm.

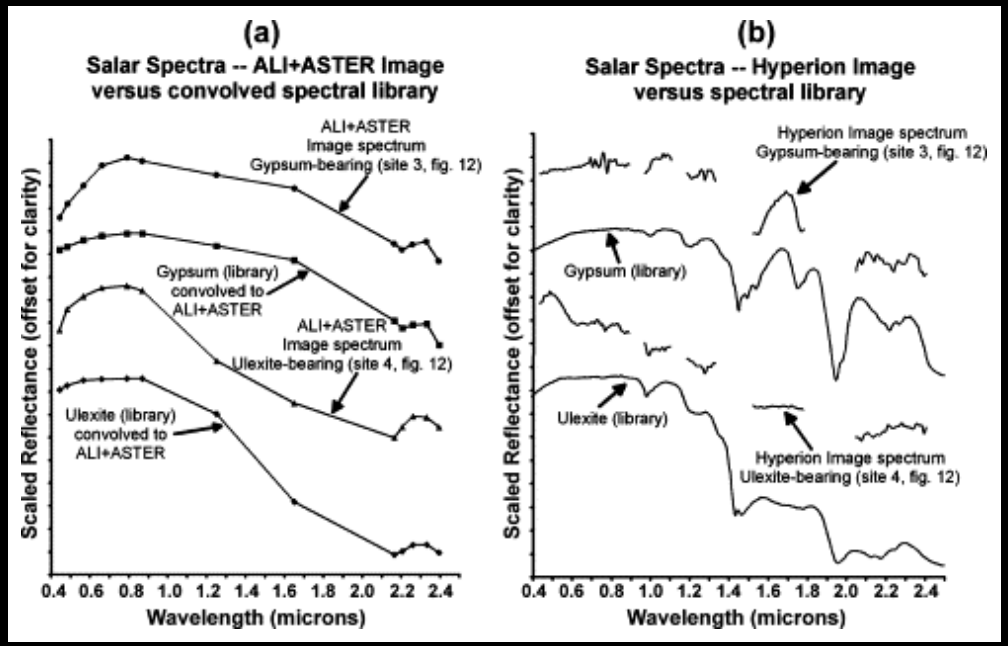

# EO-1 Hyperion Imaging of Eyjafjallajökull Volcano Eruption, April 17, 2010

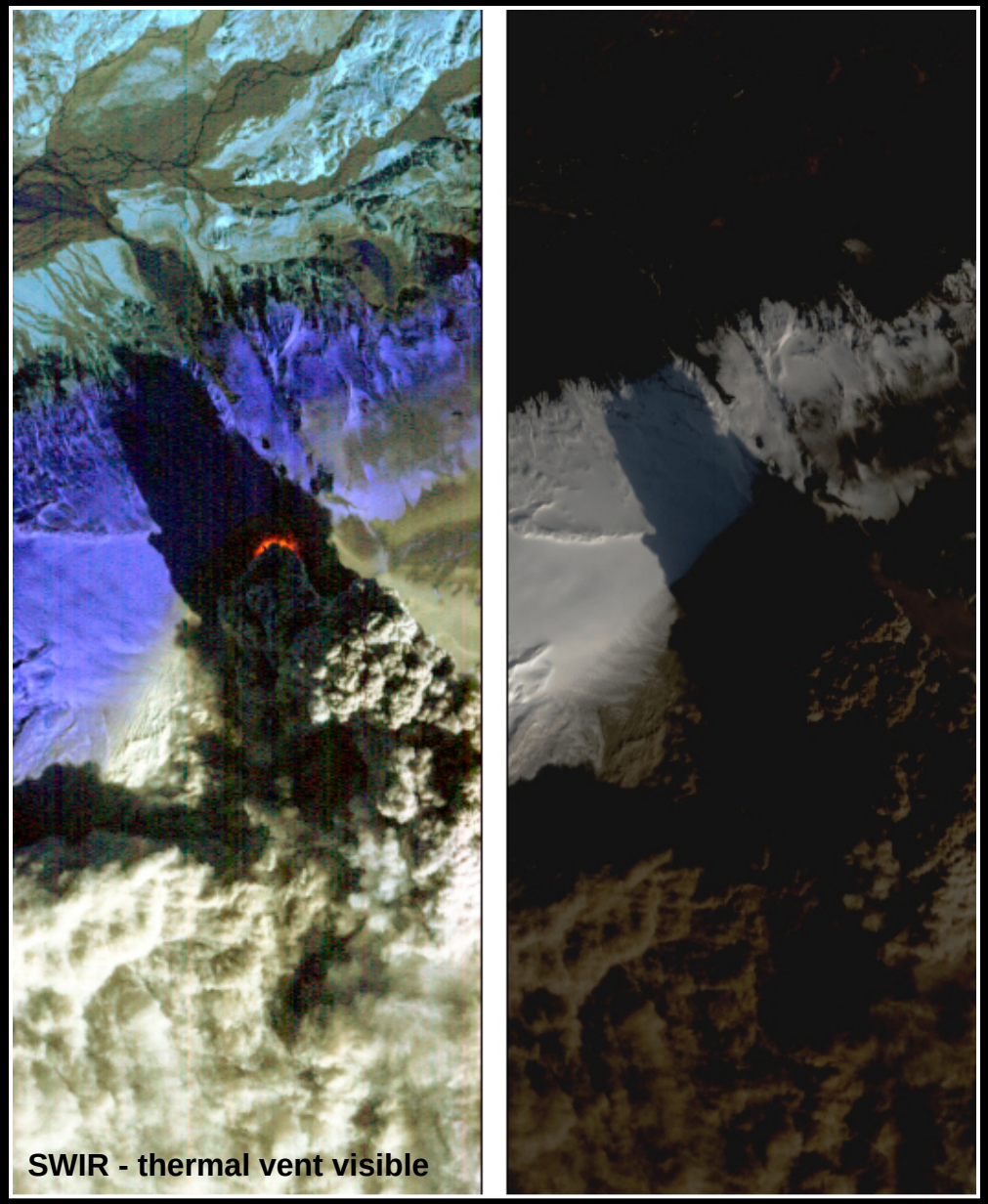


**VIS -** plumes coating everything to the South-East making the ice brown/gray

TIR imager will make daily passes at latitude of Iceland

# Hyperion Detects Sendai Fires

This image was acquired two days after the earthquake and tsunami in Sendai, Japan (March 2011). Hyperion's spectral signatures assisted in identifying surface features (a), by using the extremely high SWIR values indicative of fires (b). The ALI image (c) shows the smoke plume blowing eastward over the Pacific. In both ALI and Hyperion, the size of the fire in the Sendai harbor can be assessed, which indicates at least 5 locations with active fires, within a ≥50 pixel region (≥1500 $m^2$).

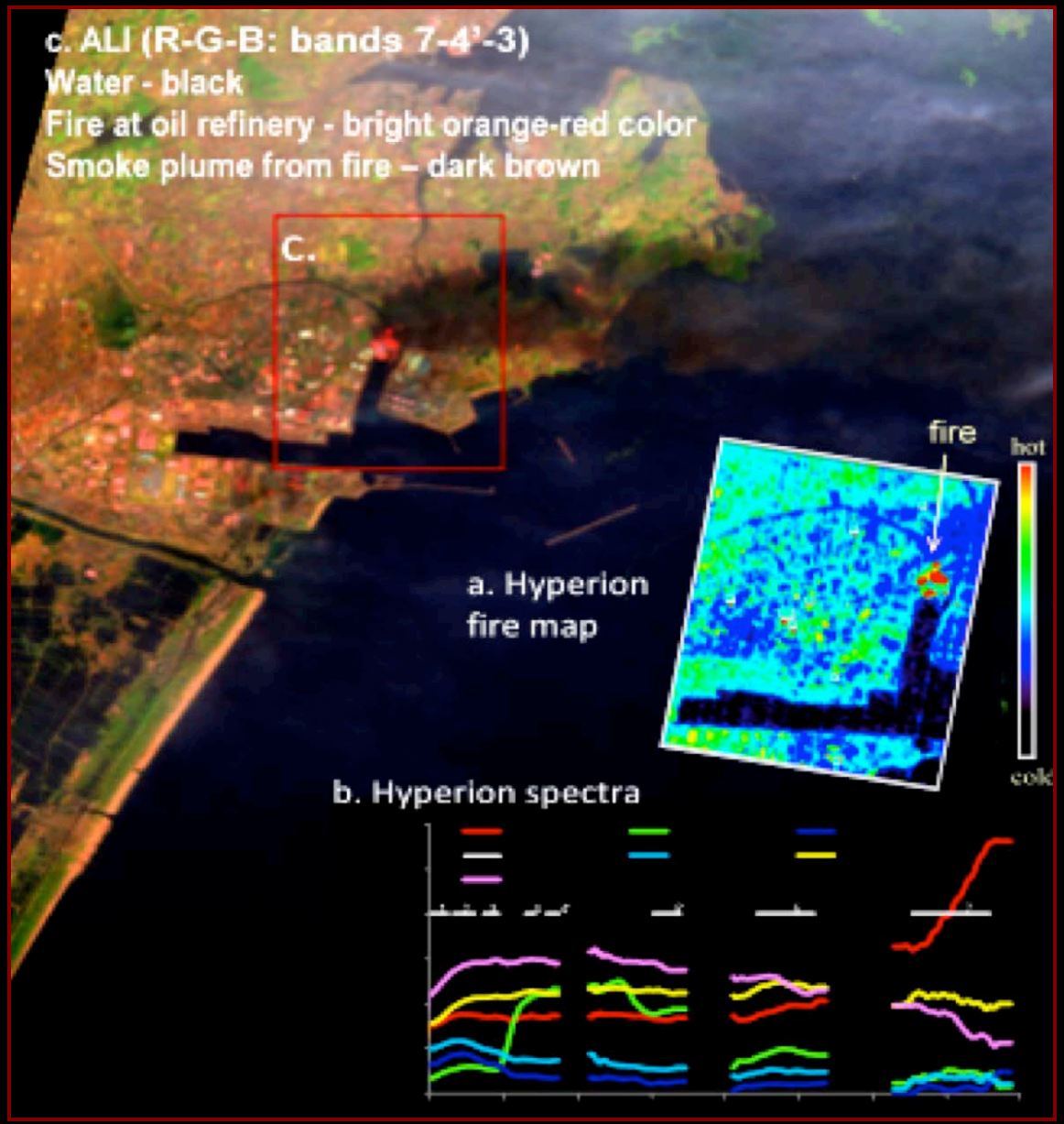

# Imaging Spectroscopy
# Measuring Species Type in Marshlands

D. Roberts, UCSB


AVIRIS Vegetation Spectra

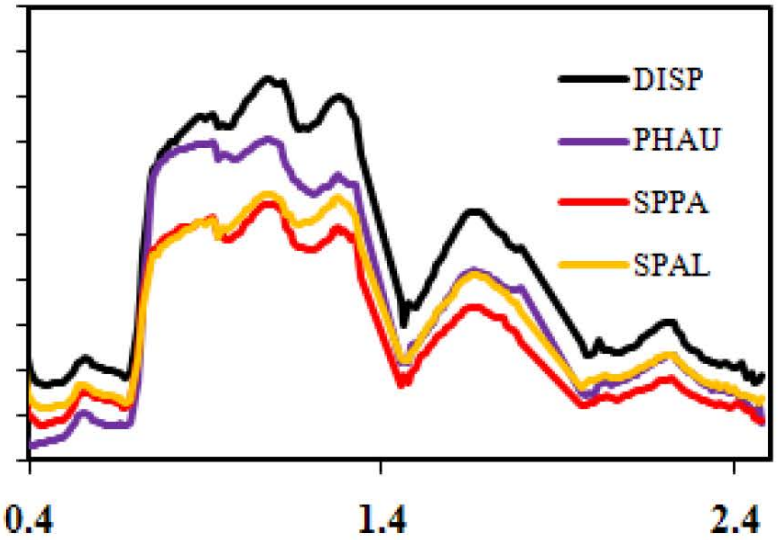


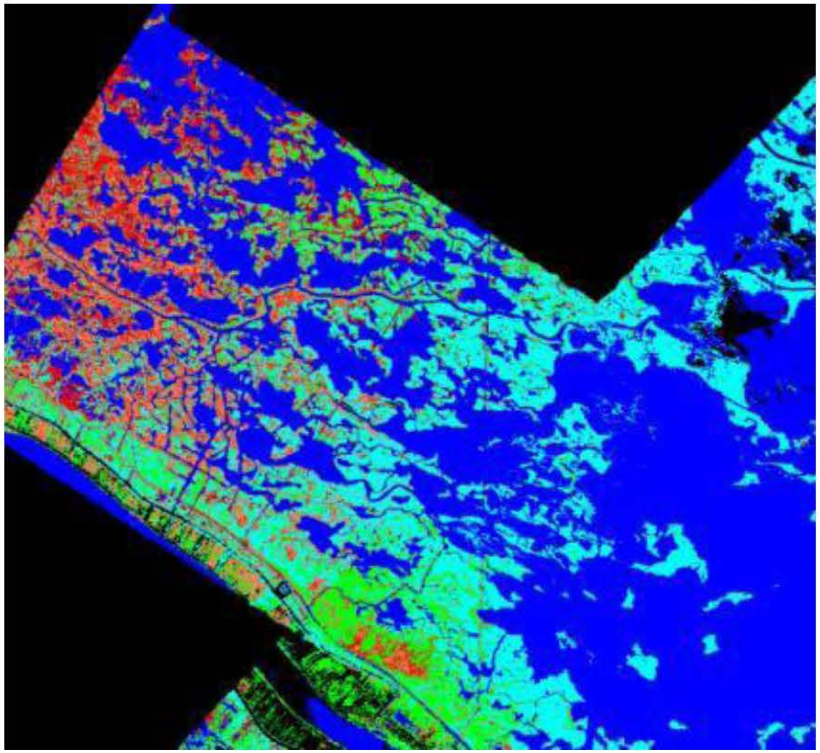

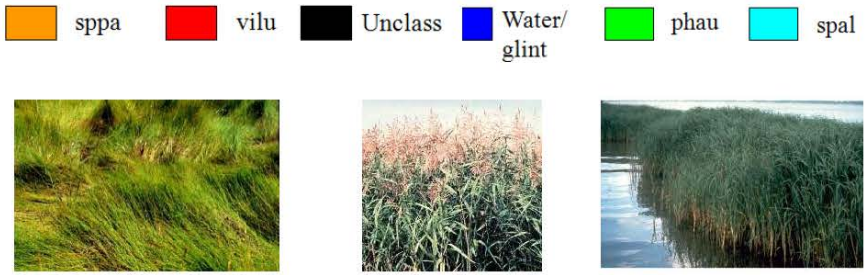


**Vegetation mapped cleanly across scene boundaries**

- ***Phragmites (phau)***
- ***Spartina alterniflora (spal)***
- ***Spartina patens (sppa)***
- ***Vigna luteola (vilu)***

True "Remote Measurement" with Spectral-Shape [Chemistry]

# Species/Functional-Type from Imaging Spectroscopy

New England, USA

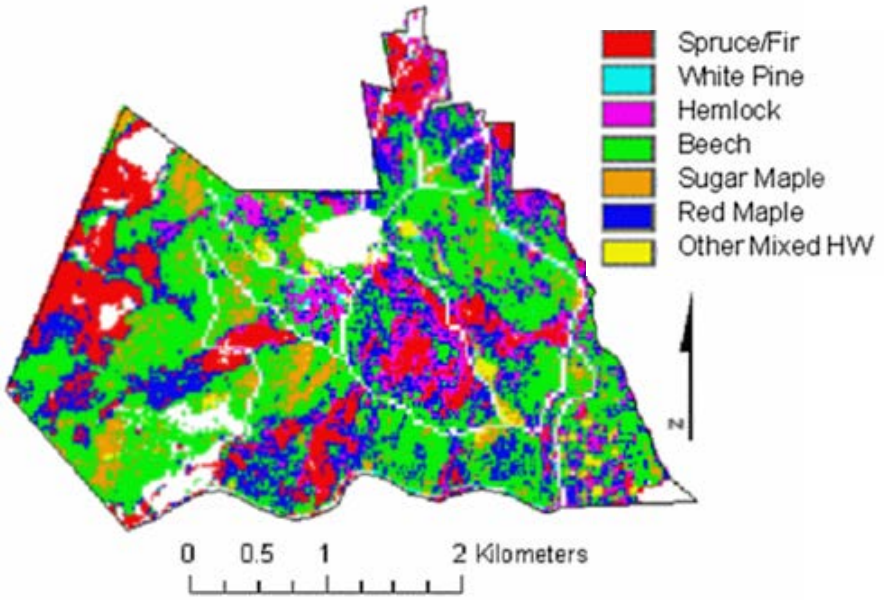


British Columbia, Canada

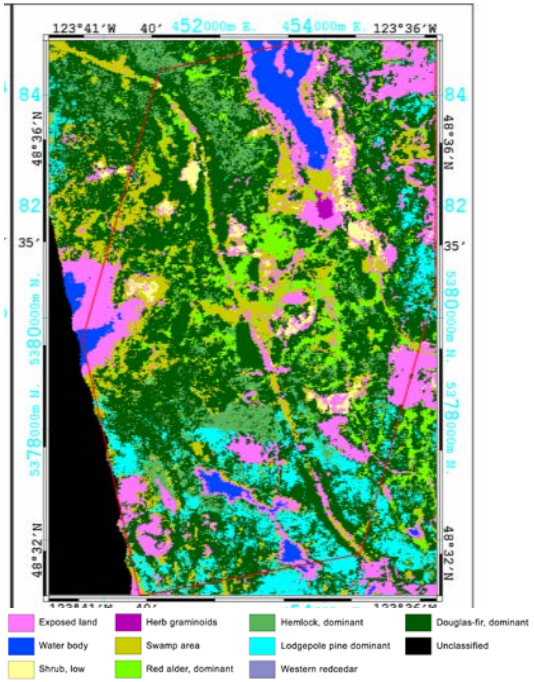


Shenandoah National Park, USA

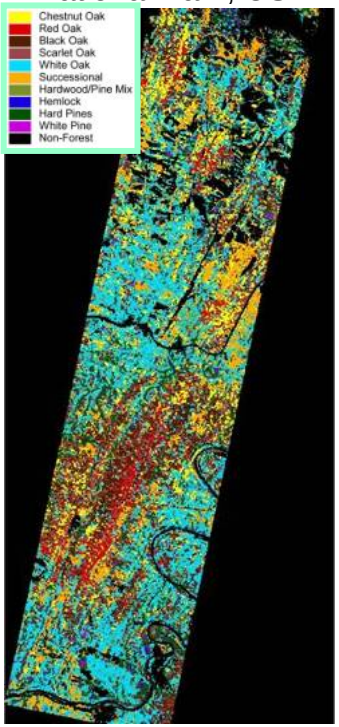


Santa Barbara, CA

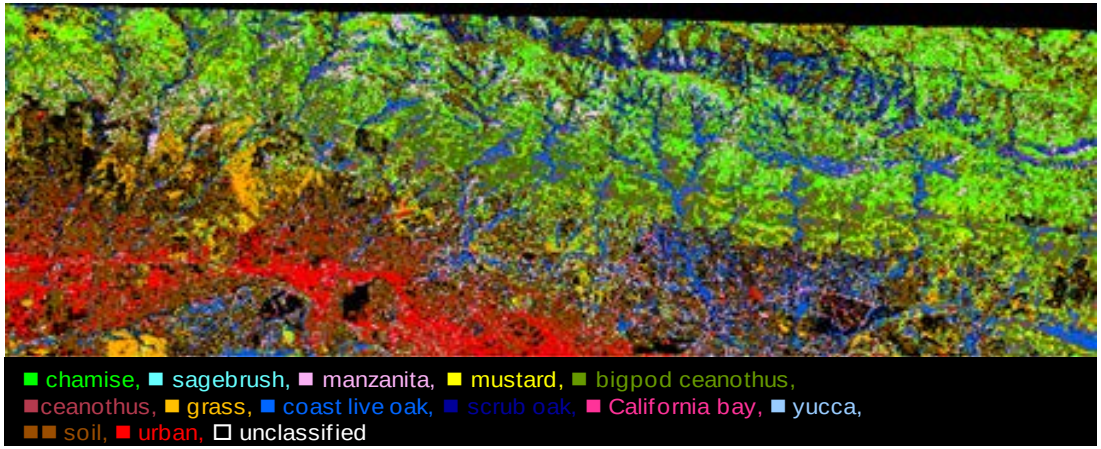


Hawaii, USA

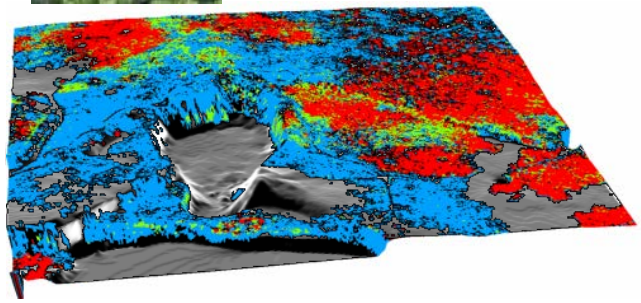

# Cover Fractions in Transition from Live/Green to Dry/Dead

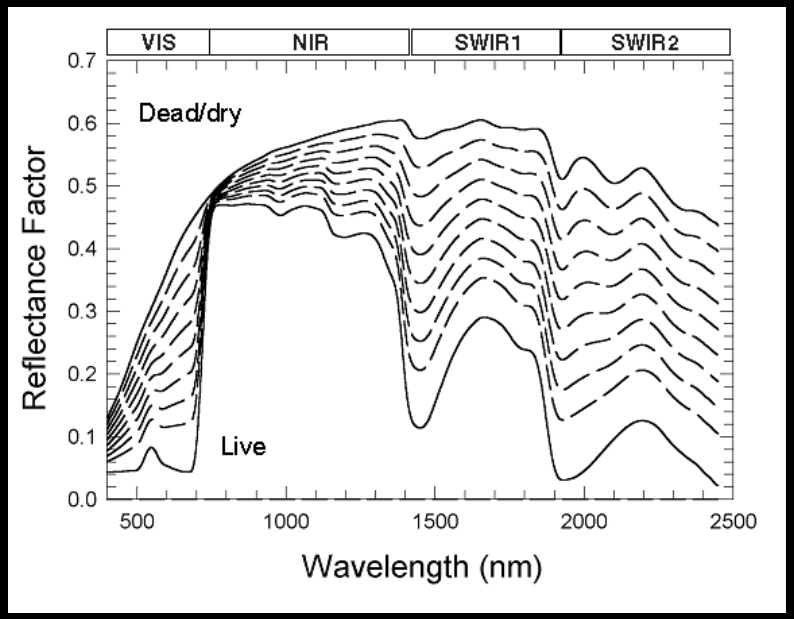


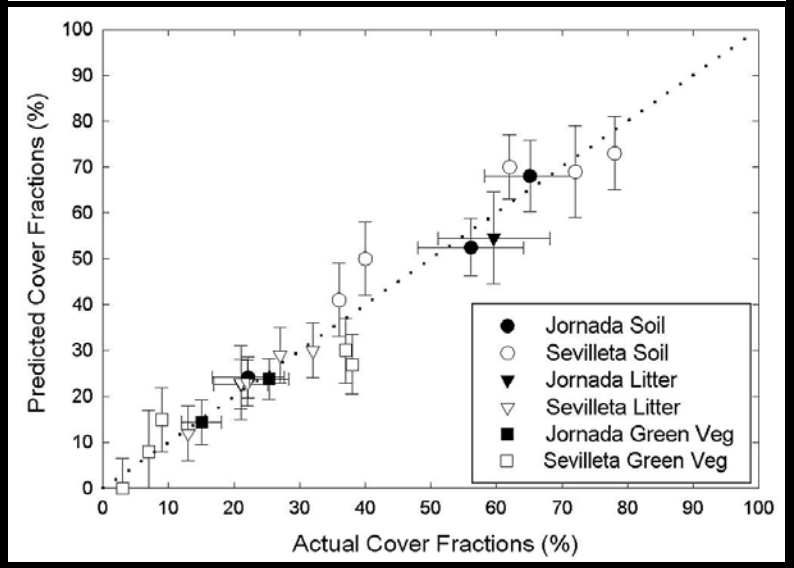


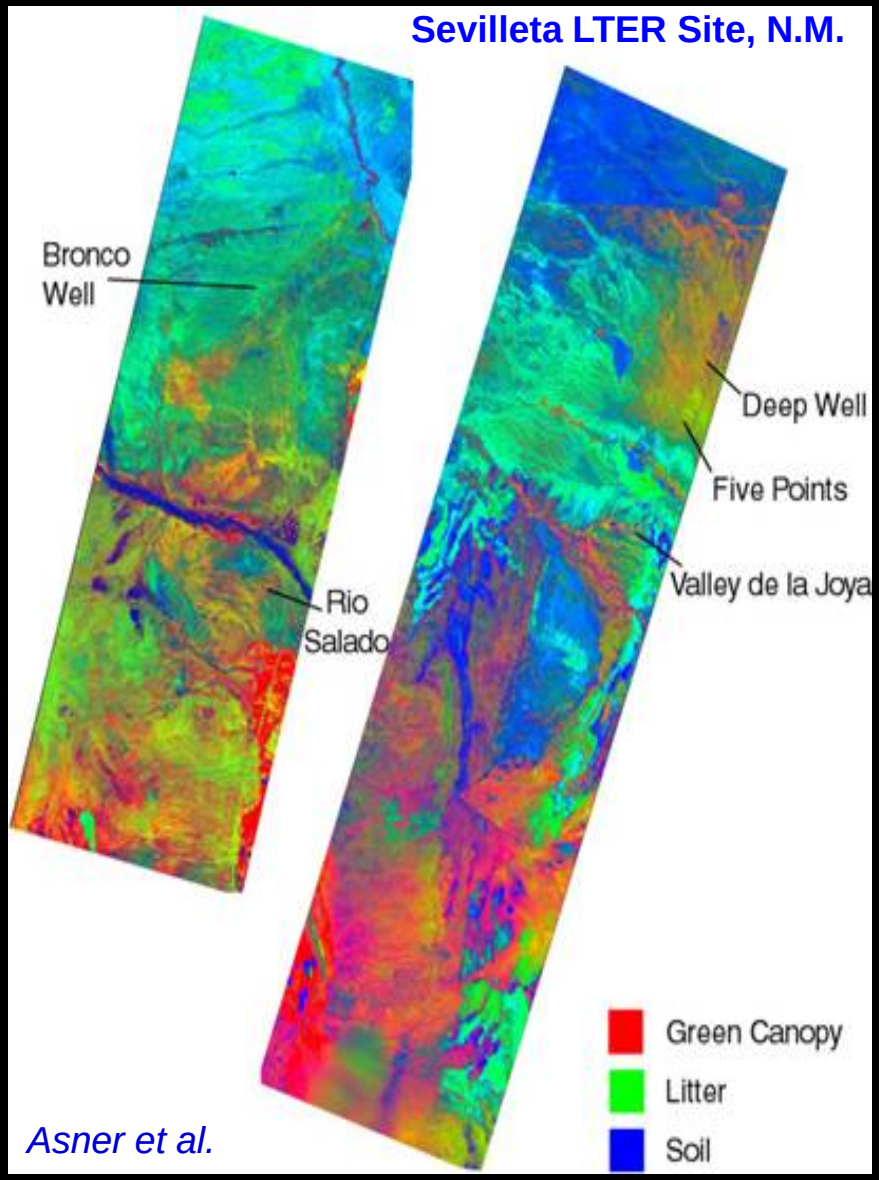

# Hyperion Distinguishes Crop Types

Detailed spectra allow greater potential for plant type identification than does Landsat

Corn–Rice–Soybean–Sunflower

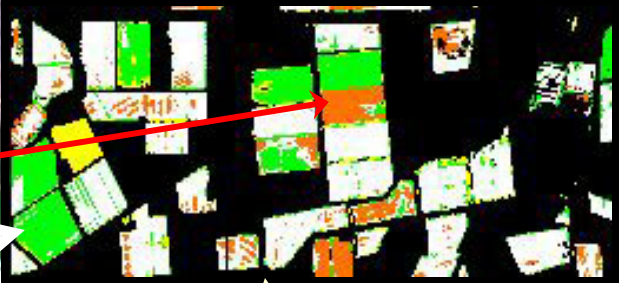


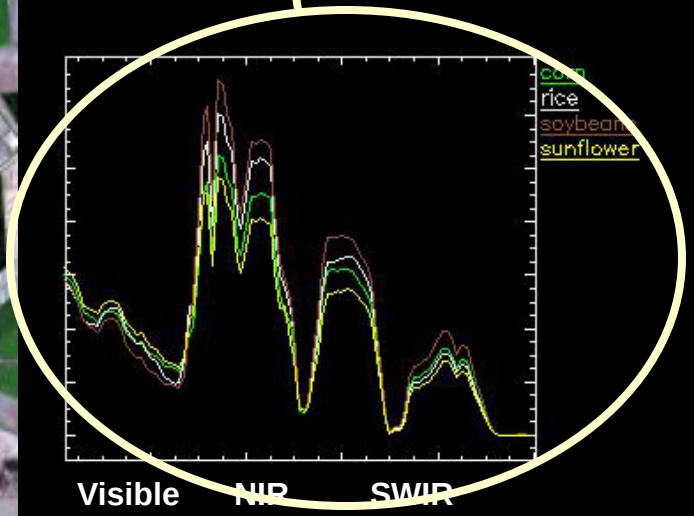

# Temporal Sequence of Hyperion Images

*Coleambally Irrigation Area (CIA), Australia*


Julian calendar day of 2001

# Spectroscopy and Agriculture

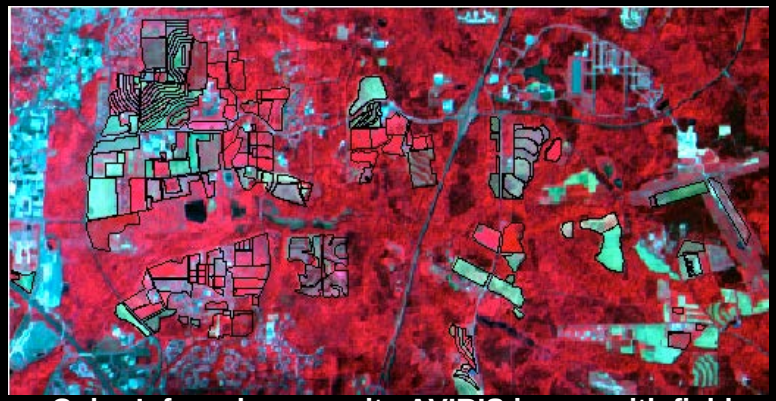

Color Infrared composite AVIRIS image with field boundaries, blue (549 nm), green (646 nm), red (827 nm)

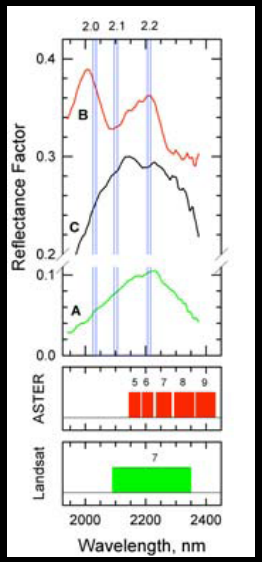


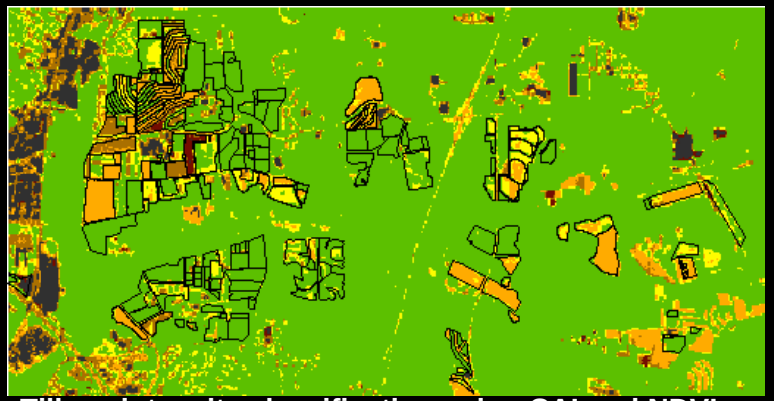

**Tillage intensity classification using CAI and NDVI**
(overall classification accuracy = 92%)

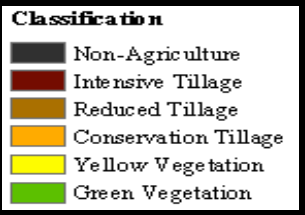


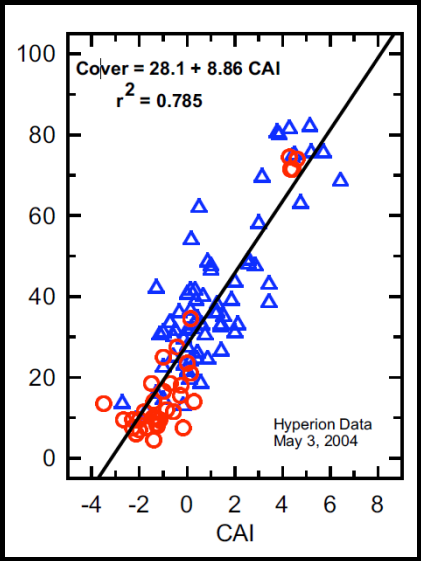


$$CAI = 0.5(R_{2000} + R_{2200}) - R_{2100}$$

Crop Residue Cover vs. CAI for Hyperion, Iowa – 5-3-2004

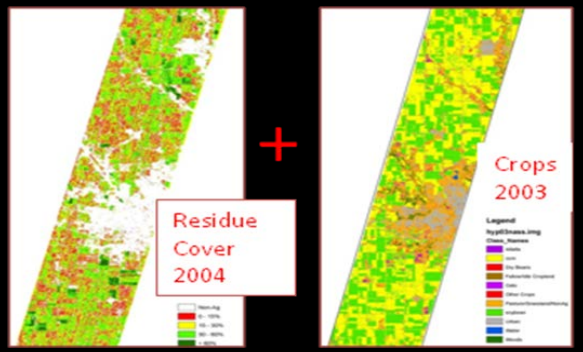


For dry and moist conditions CAI is adequate for assessing crop residue cover.

*(Daughtry et al. 2001, 2006 and 2010)*

# Hyperion Detects Canopy Water Content

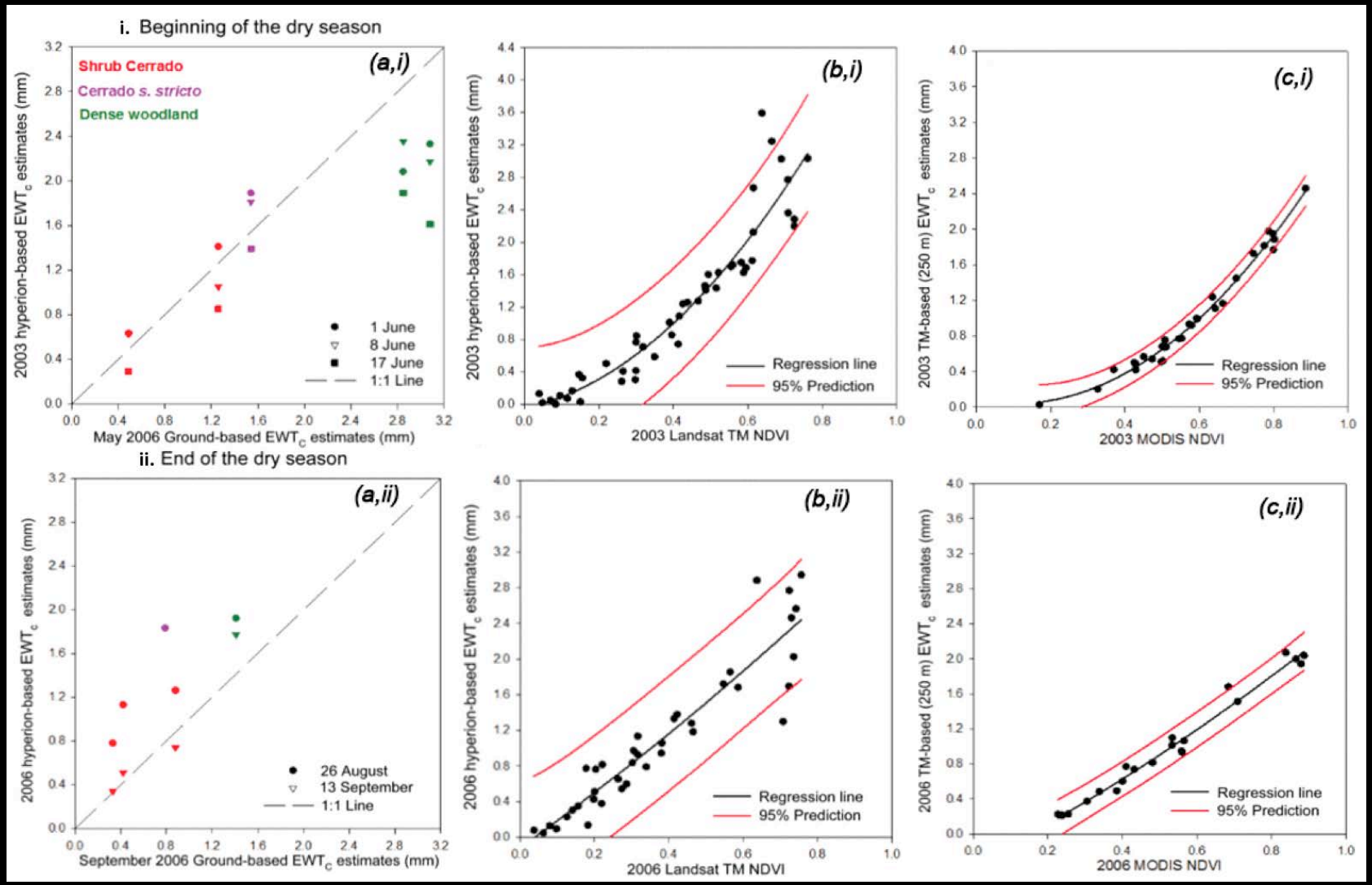


Extrapolating canopy water content (Hyperion EWTC) to regional scale: **(a)** Field measurements and Hyperion-based EWTC, **(b)** 30m TM NDVI and Hyperion-based EWTC, and **(c)** MODIS NDVI and 250m TM-based EWTC at **(i)** the beginning and **(ii)** the end of the dry season, from Ferria et al. (2011).

# Hyperion Detects Wildfires

Night-time observations allow the suppression of normally reflected light to permit the detection of emitted energy, such as fire temperature. This makes night-time fires stand out dramatically, as only the emissions from the active fires are detected. Smoke is very reflective in the daytime but can be seen through at night.

## Hyperion Image of the Tucson Wildfires – July 3, 2003

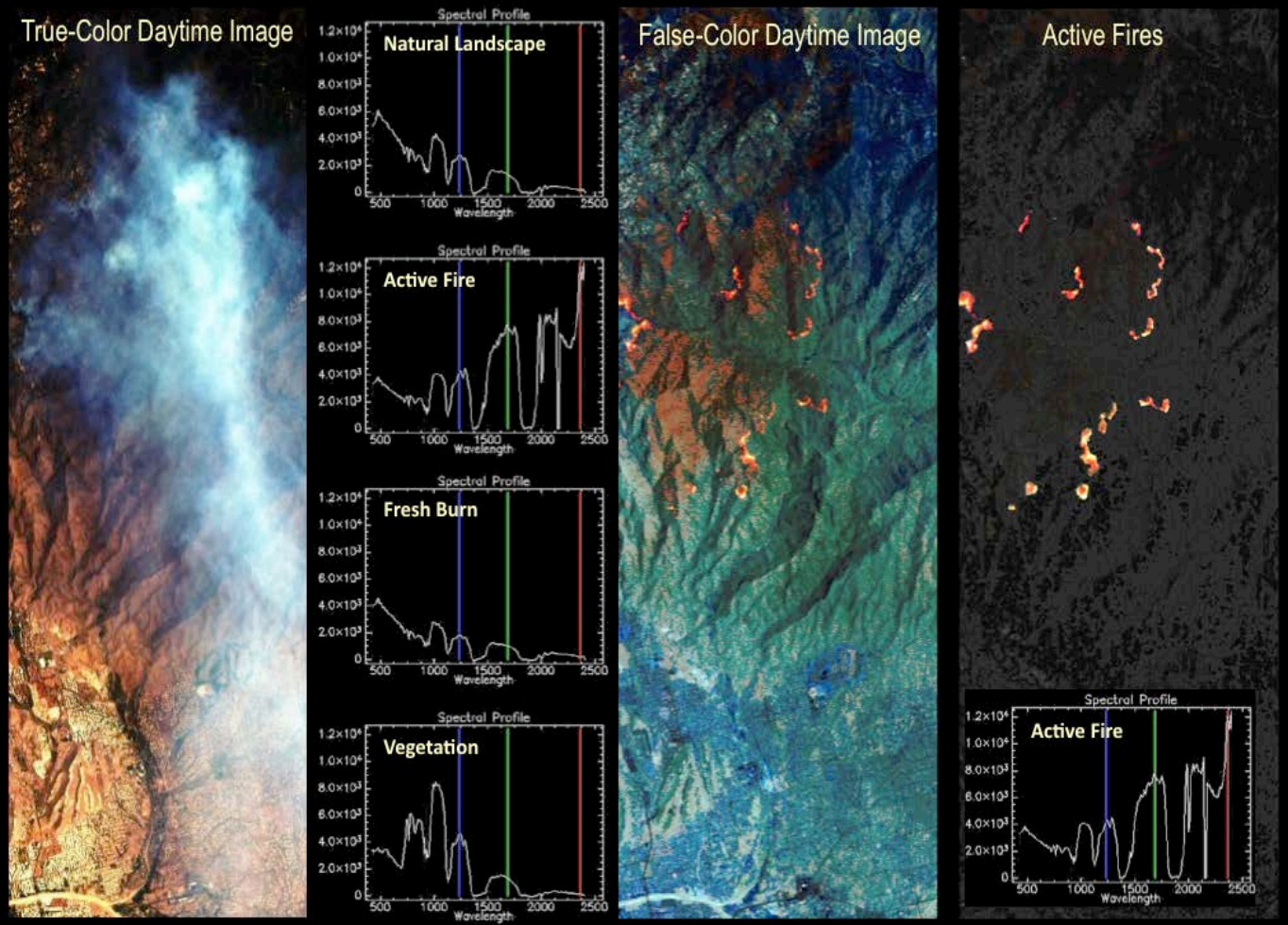

# Hyperion Detects Volcanoes

NASA's Autonomous Sciencecraft Experiment (ASE) [Chien 2005; Davies 2005] uses day and night time Hyperion observations to detect hot pixels and identify **volcanic activity**. This rapid response allows early assessment of hazard and risk.

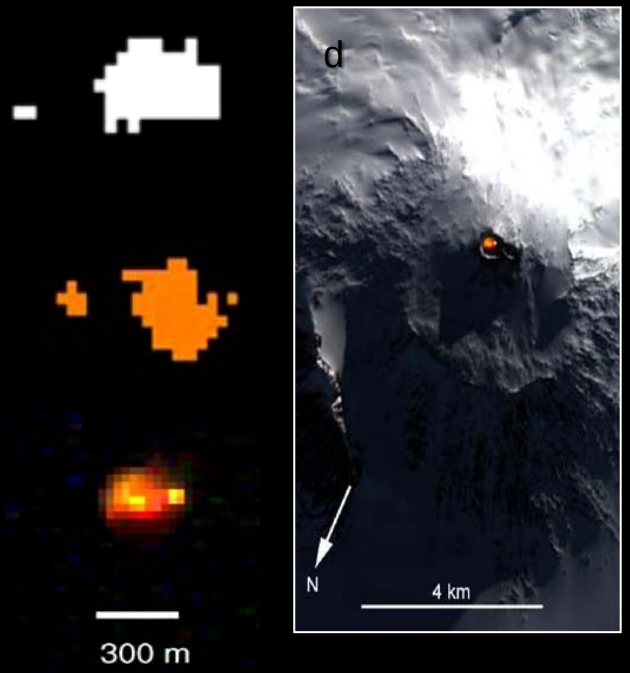


*ASE Thermal Classifier detects thermal emission from the Mt. Erebus lava lake (2004), using night and day Hyperion images to produce a L1 map of thermally active pixels. These active pixels (from night) are superimposed on a daytime image [Davies 2006].*

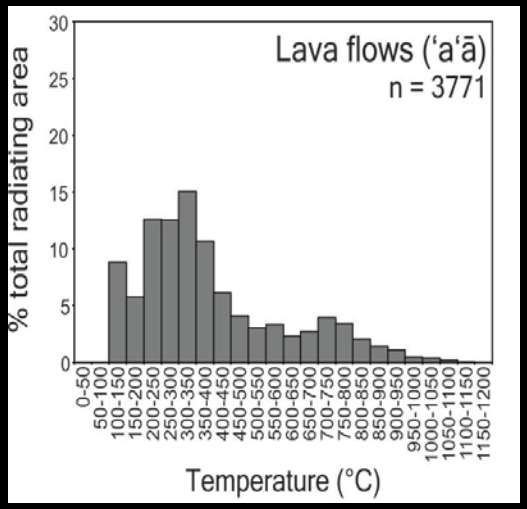


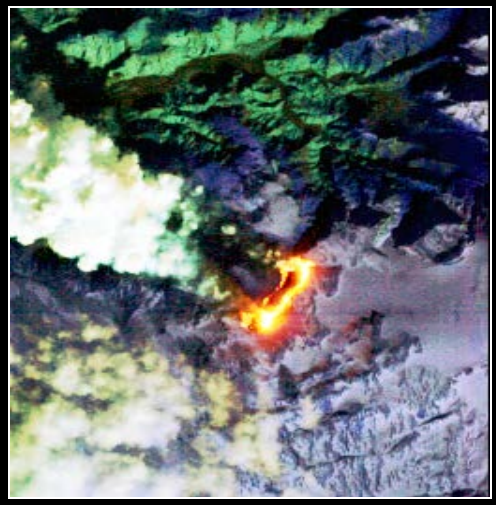

*Hyperion determines eruption type and lava chemistry on the basis of remotely sensed temperature alone (Wright 2009).*

# Eruption of Mt. Etna, Sicily

ALI Pan Enhanced Bands 3-2-1

Hyperion 7-5-4 Equiv

EO-1 ALI Bands 7-5-5'

## July 22, 2001

## Hyperion Temperatures for Etna

| Spectrum | Crust Temp | Hot Temp | Area Hot |
|---|---|---|---|
| J 13 - CTB | 346 C | 994 C | 0.0025 |
| J 13 - MM | 874 C | 876 C | 0.45 |
| J 13 - CTS | 976 C | 978 C | 0.47 |
| J 13 - TipX | 210 C | 900 C | 0.00034 |
| J 22 - MS | 726 C | 1075 C | 0.090 |
| J 22 - CX | 487 C | 1075 C | 0.022 |
| J 22 - RS* | 1054 C | 1058 C | 0.690 |

## EO-1 Hyperion Spectra

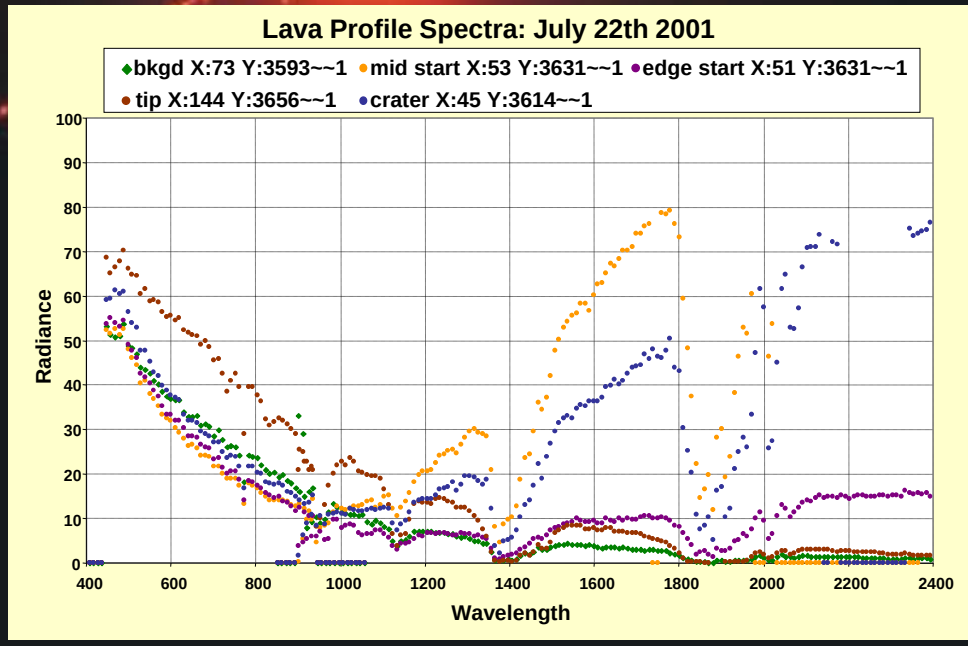

# Classification for Agatti Island, India

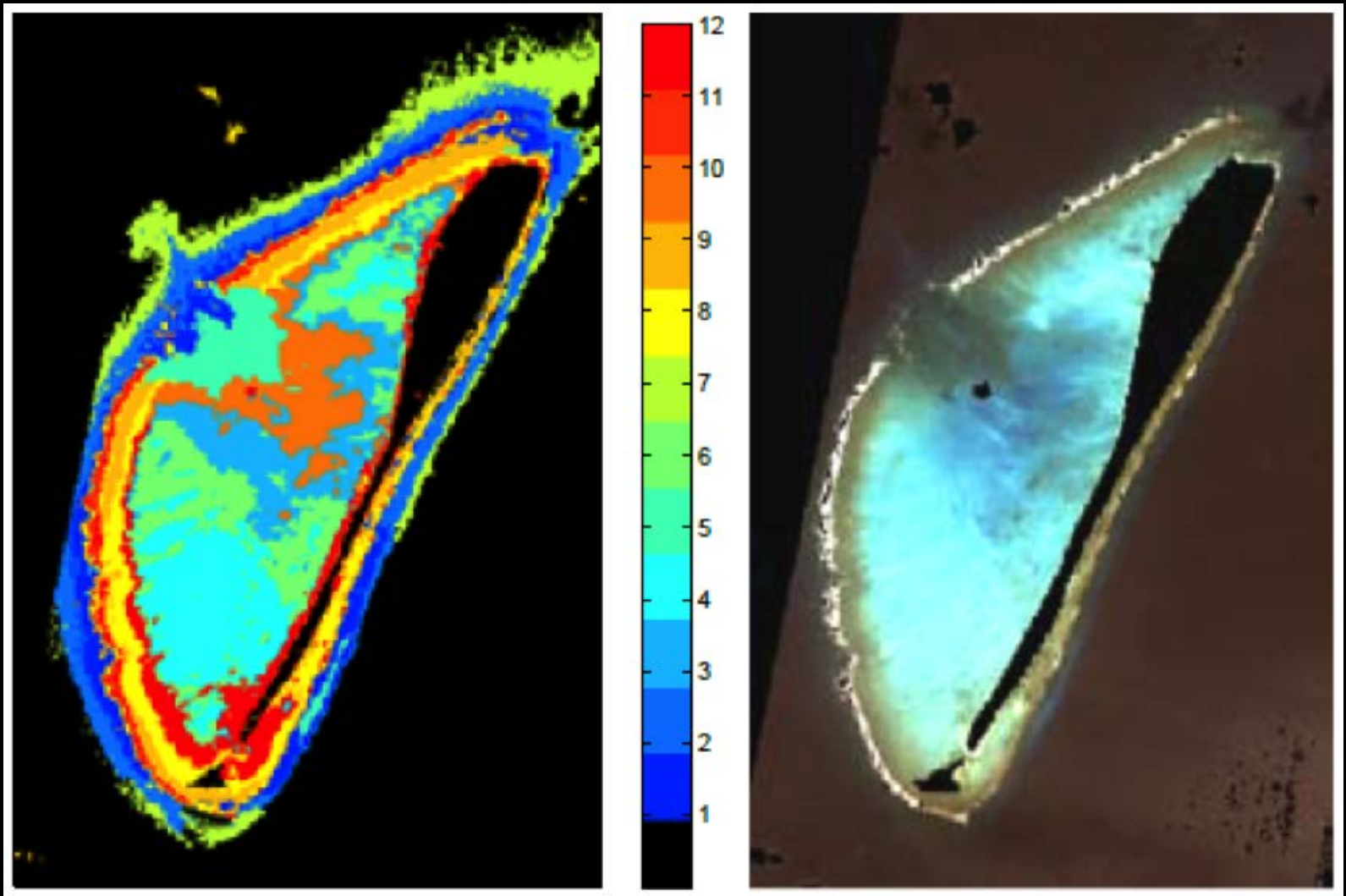


EO-1 Hyperion k-Means classification for Agatti Island, India, where the classes are represented as 1 and 2: Reef Slope; 3: Intermediate Lagoon; 4: Sand Sheet; 5 and 10: Deep Lagoon; 6 and 12: Shallow Lagoon; 7: Submerged Reef; 8, 9 and 11: Reef Flat.

# Using Hyperspectral Data to Detect Sea Grasses

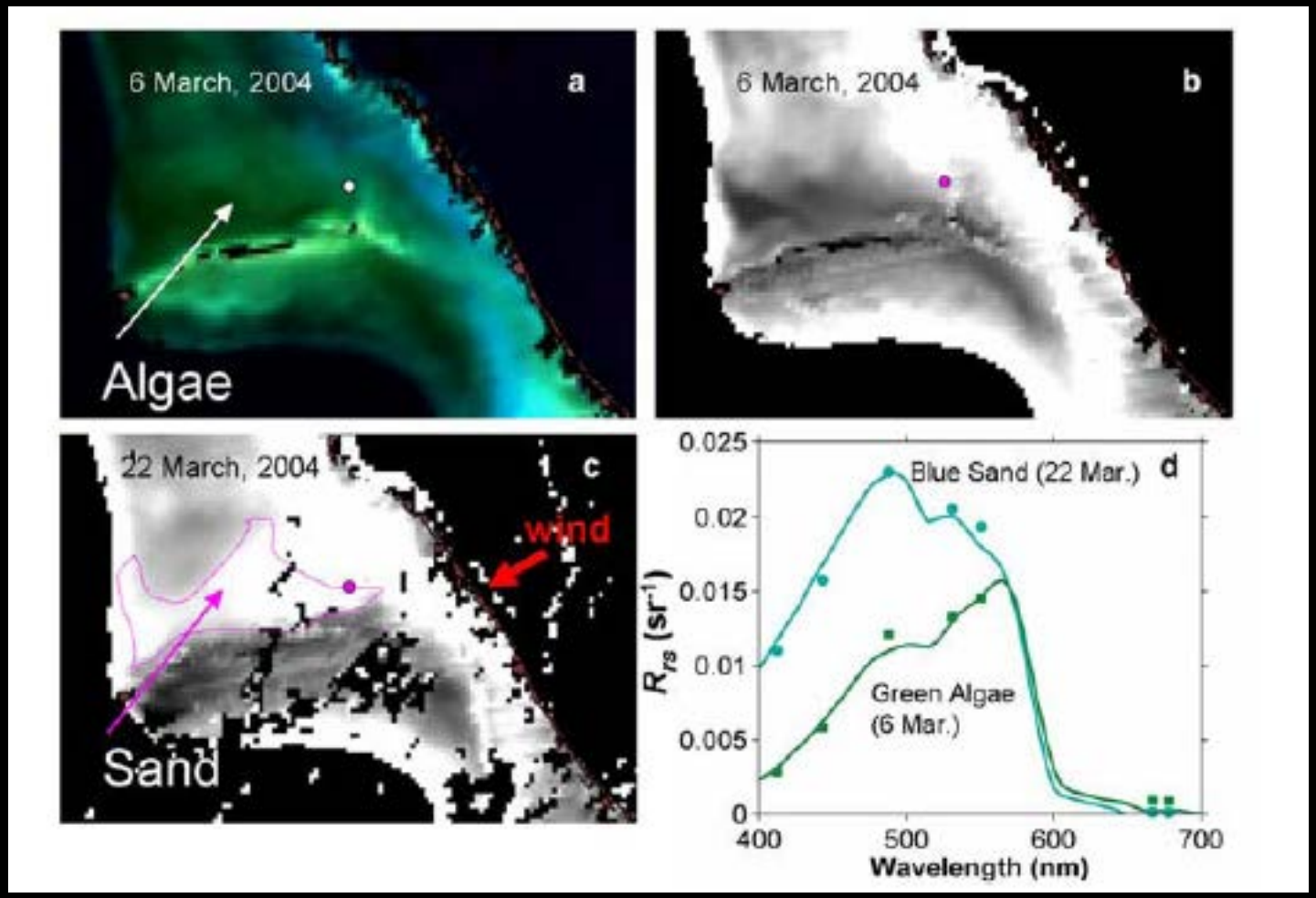


Pulsed export of >7 x$10^{10}$ g of carbon directly to seafloor (negatively buoyant). This is equivalent to the daily carbon flux of phytoplankton biomass in the pelagic tropical North Atlantic and 0.2–0.8% of daily carbon flux from the global ocean.

*Dierssen et al. 2009. Geophys. Res. Lett.*

# Hyperion Images Flood Runoff

Regarding the atmospheric correction of EO-1, we collaborate closely with Bo-Cai Gao in the use of ATREM (Naval Research Laboratory), and with T. Perkins and S.M. Adler-Golden in the use of FLAASH (Air Force Research Laboratory).

**<u>Issues</u>: When using the terrestrial approaches, the correction does not account for contributions from specular reflection at the air water interface (including sun glint and cirrus clouds).** Atmospheric correction and these issues have been discussed at the HyspIRI Symposia in 2010, 2011, and are on the agenda for the HyspIRI Symposia 2013.

*EO-1 Hyperion, October 2011 Tsunami*
*Sendai, Japan*

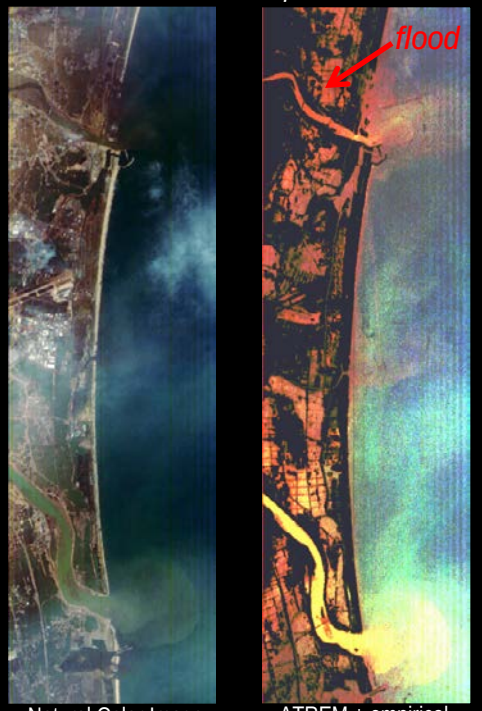


Natural Color Image

ATREM + empirical
Non-water black

**<u>Correction approaches and their relevance to Hyperion:</u>**

- The standard Cox-Munk type of sunglint model, suitable for modeling glint effects at a spatial resolution of 1 km (large pixel), is not suitable for modeling sunglint effects at the smaller 20-30 m pixels, because the individual wave facets can be seen at this resolution.
- "Image driven" and "empirical" correction procedures have been suggested (Z-P. Lee 2007, B-C. Gao 2009, Brando 2009) for use with HICO, AVIRIS, CASI-2, Hyperion, and others. An additional correction routine has been included in FLAASH (LASH, Adler-Golden 2005).
- The empirical correction approach is based on the facts that: clear ocean waters have water leaving reflectances above 0.8 μm close to zero, and sunglint and cirrus reflectances in the 0.4–1.0-μm region are spectrally constant.

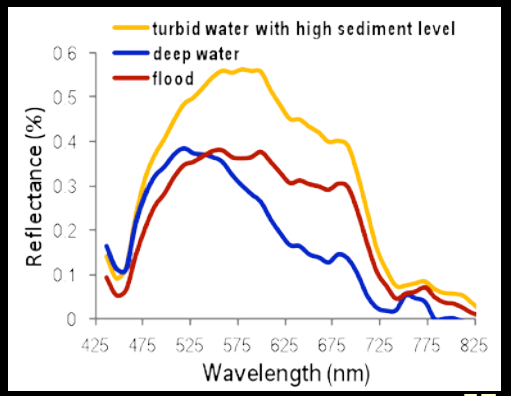


Sensor SNR has a large impact on water observation, since water targets have much weaker signal than land. Low signal levels can be a limiting factor for the implementation of the image driven empirical corrections. However, for many shallow coastal areas, due to the increased turbidity of water, and in places with strong reflectance from the bottom, the signals emanating from the water surface can be much stronger than that from open ocean waters.

# Reflectance Changes with Age Class & Species Mixtures

Wind River Canopy Crane Site, Carson, WA
Age class distributions from newly harvested to 500+ yr “old growth” Conifer Forest

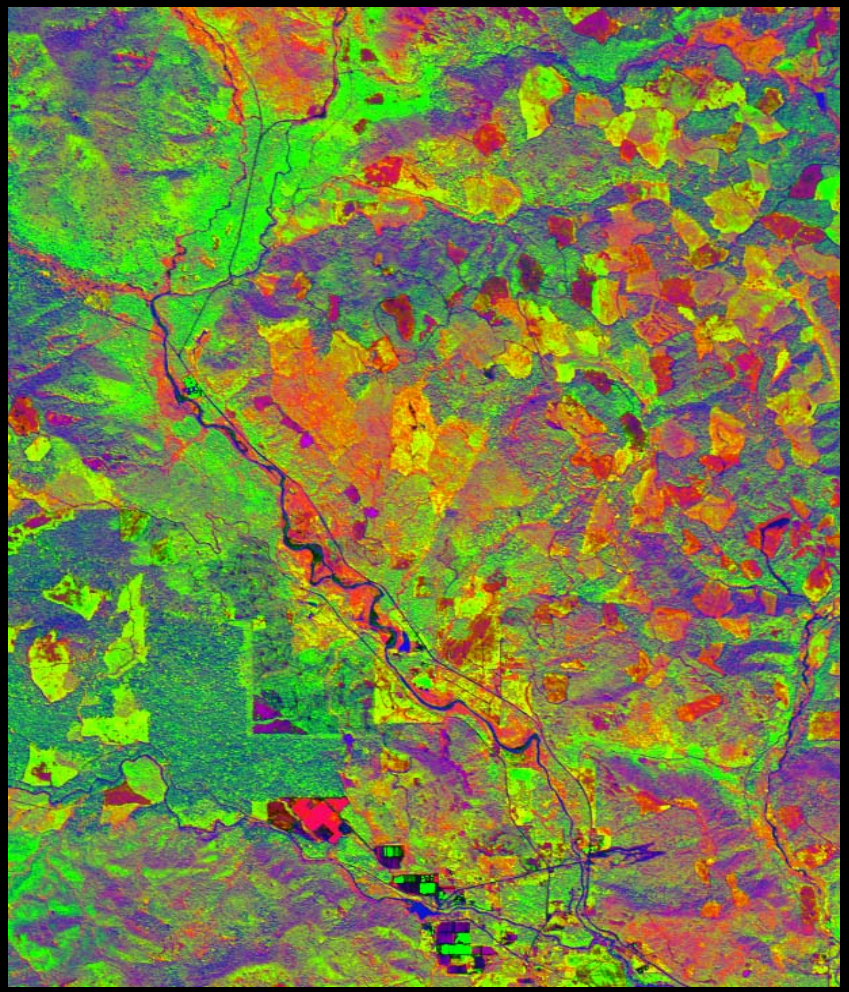

R=soil, G=vegetation, B=shade

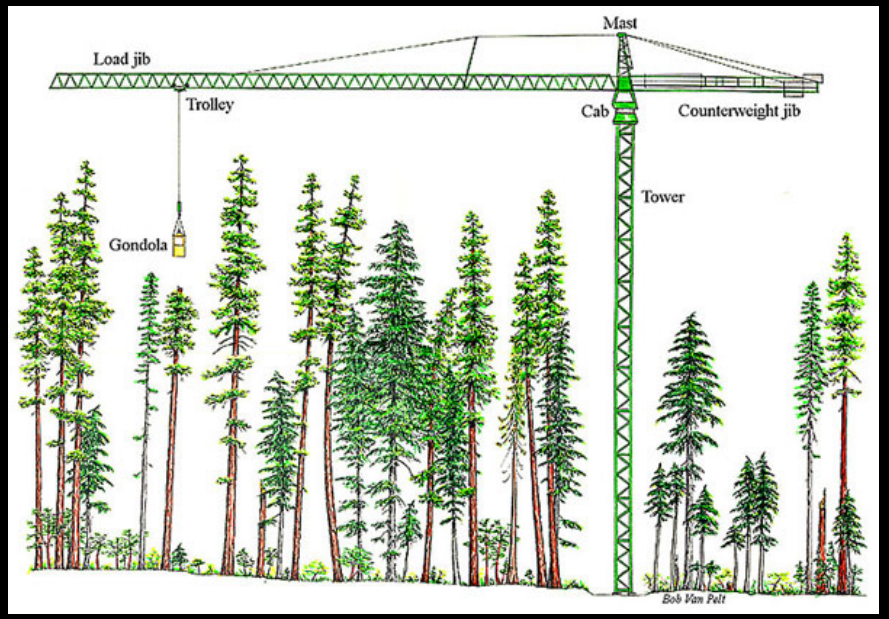


*A. Fox 2013*

# Wildfire Scars Valparaiso, Chile

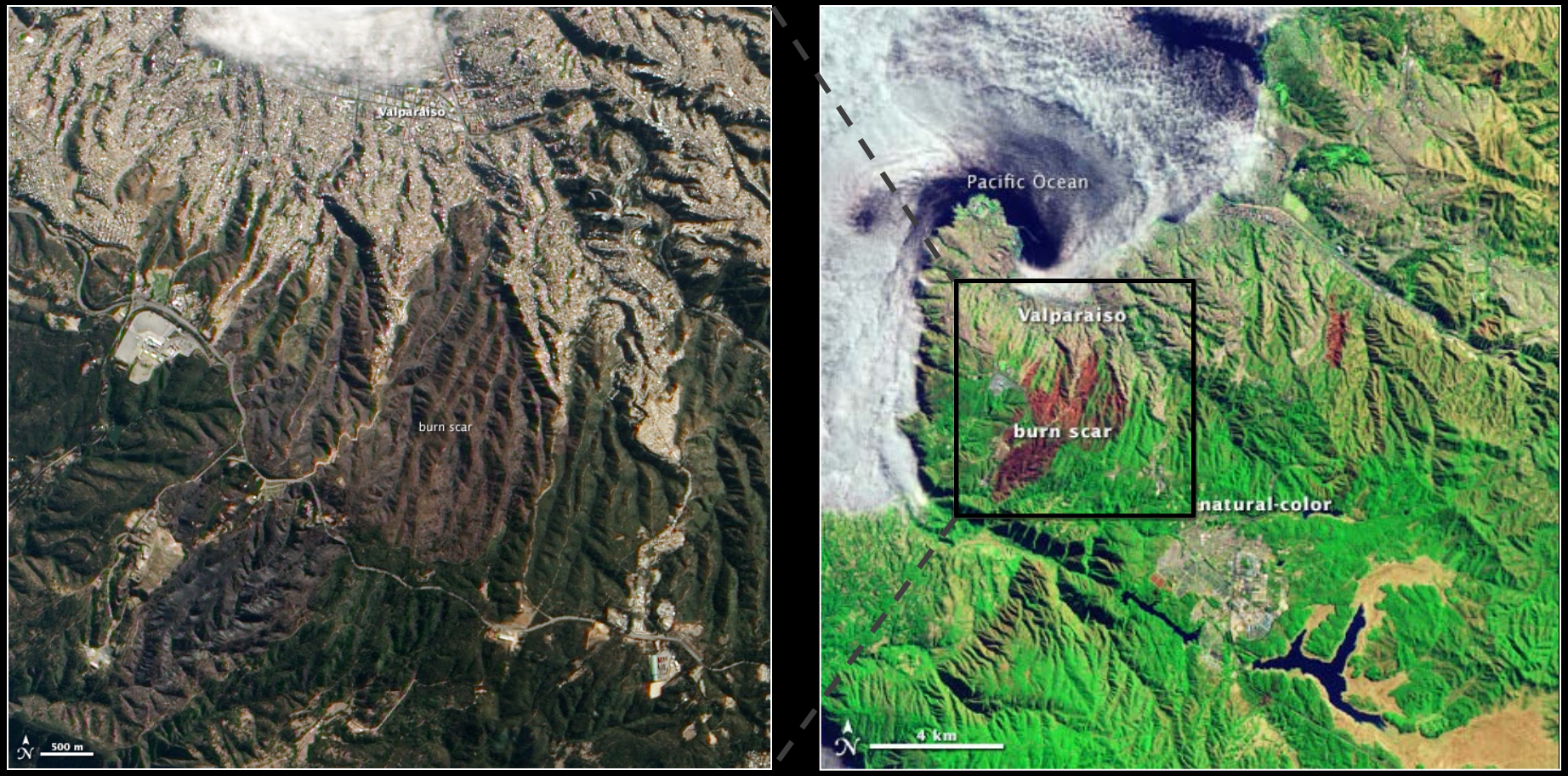


May 4, 2014
False- and True-Color Images from ALI
Wildfire Scars Valparaiso, Chile

The city of Valparaiso rises from Chile's Pacific coastal plain. On April 12, 2014, a wildfire broke out in the southern hills and quickly moved into the city: 3,309 homes were destroyed and 15 people died. On the right, a false-color ALI image shows the fire scar as dark red; plants are bright green; sparse vegetation is tan; and the city is gray and purple. The left image shows a more detailed, natural-color version of the scene: the newly burned land is dark brown and unburned vegetation is dark green.

# Chilika Lake and Nalabana Bird Sanctuary, India

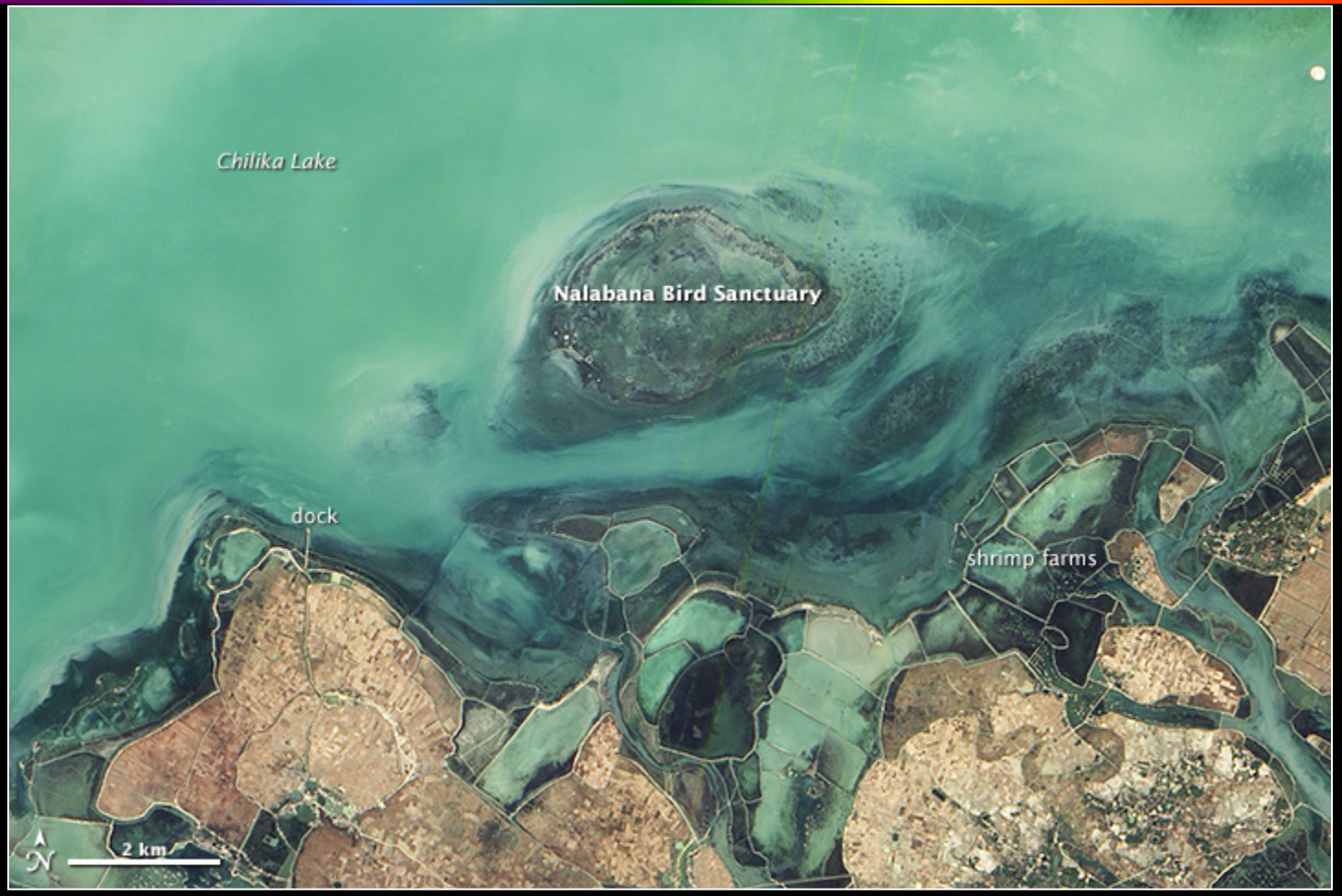


December 14, 2013
True-Color Image from ALI
Chilika Lake and Nalabana Bird Sanctuary, India

Chilika Lake is the largest lagoon in India and one of the largest in the world. The interplay between fresh water and salty tidal water gives Chilika's waters a brackish quality, with salinity varying significantly throughout the lake. These variations open up a range of ecological niches and promote a rich diversity of species.